Proposal and efficiency analysis of cascaded adiabatic frequency conversion in coupled microrings

Luis Cortes-Herrera [*], Xiaotong He, Jaime Cardenas, and Govind P. Agrawal

Institute of Optics, University of Rochester, Rochester, New York 14627, USA

Adiabatic frequency conversion (AFC) in microring resonators is a promising alternative for fully integrable and tunable frequency shifting of optical signals. Nonetheless, the magnitude of the frequency shift via simple AFC in a single ring is fundamentally limited by the material platform. To overcome this limitation, we propose and analyze a scheme to induce cascaded AFC (CAFC) along a chain of coupled, yet initially detuned rings, without requiring unloading the optical signal into a bus waveguide between successive modulations. For concreteness, we examine thoroughly the simplest nontrivial case of a chain of two rings and briefly discuss the generalization to a chain of an arbitrary number of rings. We analyze the temporal dynamics of this CAFC process using temporal coupled mode theory. We examine the transformation of the input into the frequency-shifted output as a rank-one linear operator in the vector space of finite-energy pulses. In this way we show that the energy efficiency of CAFC depends on the input pulse shape through a Schwarz inequality, just as in single-ring AFC. We propose a numerical scheme to maximize the CAFC efficiency with respect to the process's timescales and discuss the physics involved. We show that the resulting CAFC efficiency converges in a polynomial manner to a maximum as the process becomes progressively idealized. Furthermore, we show that this maximum efficiency is identical to that for single-ring AFC, e.g., 0.7951 for a symmetric, single-lobe input pulse. Thus, we show that CAFC can become more efficient than multiple instances of single-ring AFC. We explain the polynomial convergence of the CAFC efficiency as a consequence of its real analyticity as a function of the process's timescales under our scheme. We leverage this polynomial convergence to model the CAFC efficiency as a simple polynomial in few normalized timescales. We then utilize this polynomial model to predict optimal values for the remaining free parameters and the scaling of the CAFC with the interring detuning.

I. INTRODUCTION

In photonics, frequency conversion is usually realized via nonlinear wave mixing. In recent years, the advent of integrated photonics has enabled broadband wave mixing on a chip with a compact footprint [1–4]. Despite its successes, nonlinear wave mixing has several inherent limitations [5–7]. First, it demands a high-power optical pump, which impedes on-chip integration. Second, nonlinear wave mixing obeys conservation of photon energy. Consequently, to tune the output frequency, one must change the input frequency or the pump frequency. Third, efficient wave mixing requires phase matching, which restricts both the waveguide geometry and the range of possible output frequencies.

Adiabatic frequency conversion (AFC) is a promising alternative for frequency shifting of optical signals. AFC is the phenomenon in which light excites a resonant mode of an optical cavity, the cavity's refractive index is temporally modulated, and the light follows the cavity's instantaneous resonance frequency [8,9]. This process is called adiabatic because it was shown numerically in its first investigations [9] that it preserves the adiabatic invariant of a harmonic oscillator [10,11]. In contrast to nonlinear wave mixing, AFC does not require optical pumping or phase matching and is not restricted by photon-energy conservation. Moreover, its output frequency can be tuned by adjusting the magnitude of index modulation within the cavity. As a result, AFC can be used to realize on-chip, tunable frequency conversion. AFC has been demonstrated through injection of charge carriers in silicon cavities [12–16] and in semiconductor-based metasurfaces [17], through the optical Kerr effect in a silica toroidal cavity [18], and through the Pockels effect in bulk [19] and integrated [20] lithium-niobate resonators.

Until recently, most theoretical work on AFC has focused either on its modeling and description [8,9,21–23] or on its proposal for novel applications [8,24–26]. Analysis of the engineering of AFC in integrated photonics has only recently attracted attention. It was found in Ref. [27] that AFC of a Gaussian pulse in an all-pass resonator (e.g., a microring coupled to a bus waveguide) can yield an energy efficiency of up to 74%. In Ref. [28] we investigated the fundamental limits of AFC efficiency in a single all-pass resonator employing temporal coupled-mode theory (TCMT) [29–33]. There we demonstrated that the process's efficiency is limited by a Schwarz inequality. Consequently, near-unity efficiency can be attained only when two conditions are satisfied. First, the intrinsic loss of the resonator must be small compared to the input pulse's bandwidth and the bus-resonator coupling rate. Second, in accordance with the matched-filter principle [34,35], the incident pulse must resemble the ring's time-reversed impulse response, in this case, a truncated increasing

*lcortesh@ur.rochester.edu

exponential. Hence, for a symmetric, single-lobe pulse (such as a Gaussian pulse), relevant for optical telecommunications [5,36], the maximum AFC efficiency is limited to less than 80% [27,28]. To overcome this efficiency limit, we proposed in Ref. [37] to induce AFC over two coupled rings simultaneously, rather than a single ring. We analyzed the AFC in this system again employing TCMT. We showed that the two-ring system can achieve an efficiency of 97% for symmetric, single-lobe pulses. To explain this higher AFC efficiency, we analyzed two-ring AFC as a linear operator of rank two in the vector space of finite-energy pulses and examined its singular value decomposition.

In this paper we propose and analyze the energy efficiency of a new photonic circuit for AFC which increases the frequency shift possible in a given material platform. As is well known [9,12,20,23], the magnitude of the frequency shift $\Delta\omega$ induced by AFC in a single optical resonator is given by $\Delta\omega = -\omega(\Delta n)/n$, where ω is the resonator's original resonance frequency; n, the resonator's original refractive index; and Δn, the change in the refractive index induced via modulation. Thus, the frequency shift $\Delta\omega$ attainable via AFC in a single ring is limited by the magnitude of the modulation Δn. To increase the frequency shift of the output signal, one could induce single-ring AFC twice in succession. This process, though, is fundamentally energy inefficient. This is a consequence of the mismatch between the shape of the output of the first single-ring AFC and that of the ideal input for the second single-ring AFC [28]. In this work we propose to induce AFC in cascade over a chain of coupled, yet initially detuned microrings; i.e., to induce cascaded AFC (CAFC). With this architecture, we can subject an optical pulse to AFC multiple times in succession, without unloading the pulse into a bus waveguide between modulations. Thus, we show that CAFC can achieve higher energy efficiency than simply inducing single-ring AFC twice in series. For concreteness, we examine thoroughly the simplest nontrivial case of a chain of two rings, and briefly discuss the generalization to a chain of an arbitrary number of rings.

In Ref. [37] we also proposed to induce AFC over two coupled rings. Nonetheless, in that scheme, AFC is induced simultaneously over two resonant rings, rather than in cascade over two initially detuned rings. The objective of the scheme in Ref. [37] is to increase the energy efficiency of one instance of AFC. The objective of this paper's scheme is to increase the net frequency-shift magnitude, without significantly compromising the process's net energy efficiency.

The rest of the paper is organized as follows. In Sec. II we introduce the two-ring photonic circuit we propose to realize CAFC, and we describe its operation. We present the TCMT equations governing it and write their analytical solution for strong and fast temporal modulation. In Sec. III we discuss in detail a sample CAFC process for a symmetric, single-lobe optical pulse. There we examine the temporal dynamics of the energy in each ring and the power of the resulting frequency-shifted signal. In Sec. IV we analyze the transformation of the input into the frequency-shifted output as a linear operator in the vector space of finite-energy pulses. We show that this operator is effectively of rank one, so the efficiency of CAFC is limited by a Schwarz inequality, similar to the case of simple, single-ring AFC [28]. In Sec. V we explain the
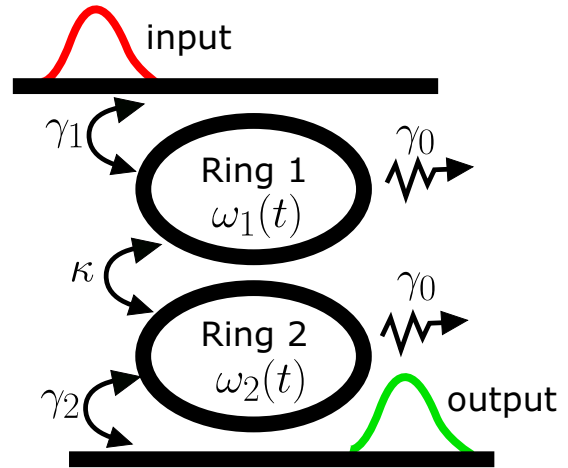

FIG. 1. Schematic diagram of the photonic circuit proposed for cascaded adiabatic frequency conversion.

numerical scheme we employ to practically optimize CAFC over the multiple timescales of the process. We discuss the physical processes which govern the optimal values of these timescales. In Sec. VI we study how the CAFC efficiency converges to its theoretical maximum as it becomes progressively idealized, as measured by three distinct timescale ratios. We find that the CAFC of our scheme has an identical limit as that of single-ring AFC, e.g., of 0.7951 for a symmetric, single-lobe input pulse [28]. Thus, CAFC can become more efficient than multiple instances of single-ring AFC in series. We show that the CAFC efficiency has a polynomial dependence on these ratios. We explain this polynomial dependence as a consequence of the CAFC efficiency being a real-analytic function of the TCMT parameters. In Sec. VII we leverage the polynomial convergence identified in Sec. VI to model the CAFC efficiency as a polynomial function of the free timescale ratios. We utilize the simplicity of this polynomial model to optimize the CAFC efficiency over the remaining free TCMT parameters and to predict its rate of convergence with respect to the interring detuning. In Sec. VIII we present the paper's conclusions.

II. DESCRIPTION OF THE PHOTONIC CIRCUIT AND COUPLED-MODE EQUATIONS FOR CAFC

In Fig. 1 we present a schematic diagram of the photonic circuit we propose to realize CAFC. It consists of two microrings evanescently coupled to each other, and each coupled to a different bus waveguide. One of the bus waveguides carries the input optical pulse, and the other, the output frequency-shifted pulse. The ring coupled to the input bus is labeled as Ring 1, and the ring coupled to the output bus, as Ring 2. The rings' refractive indices are modulated in time so that that Ring j has a time-dependent instantaneous resonance frequency $\omega_j(t)$ ($j = 1, 2$).

We assume that the input pulse is resonant with Ring 1 before frequency modulation, and that the input's bandwidth, interring coupling, bus-ring coupling, and the maximum frequency modulation are all small compared to the rings' free spectral range. Then we may describe the temporal dynamics

of the fields in this resonant system using TCMT [29–31,33]. Accordingly, the field in Ring j at time t is proportional to the amplitude $a_j(t)$ and the ring's energy equals $|a_j(t)|^2$. Analogously, the amplitude of the input (output) pulse at time t is proportional to $s_{\text{in}}(t)$ [$s_{\text{out}}(t)$], and its instantaneous power equals $|s_{\text{in}}(t)|^2$ [$|s_{\text{out}}(t)|^2$]. In agreement with TCMT, the two-component column vector $a(t) = (a_1(t), a_2(t))^T$ and the output $s_{\text{out}}(t)$ evolve in time according to

$$\frac{\mathrm{d}a}{\mathrm{d}t} = -iH(t)a + k_{\text{in}}s_{\text{in}}(t),$$

$$s_{\text{out}}(t) = k_{\text{out}}^{\dagger}a(t). \tag{1}$$

Here $H(t)$ is a time-dependent 2×2 matrix, while k_{in} and k_{out} are two-component column vectors. $k_{\text{out}}^{\dagger}$ denotes the adjoint of k_{out}. Correspondingly, the matrix $H(t)$ and the vectors k_{in} and k_{out} are of the form

$$H(t) = \begin{pmatrix} \omega_1(t) - i\gamma_1 & \kappa_{12} \\ \kappa_{21} & \omega_2(t) - i\gamma_2 \end{pmatrix},$$

$$k_{\text{in}} = \begin{pmatrix} \sqrt{2\gamma_{1e}} & 0 \end{pmatrix}^T,$$

$$k_{\text{out}} = \begin{pmatrix} 0 & \sqrt{2\gamma_{2e}} \end{pmatrix}^T. \tag{2}$$

As stated above, $\omega_j(t)$ is the instantanous frequency of Ring j. The rate γ_j is the total decay rate of Ring j; and κ_{jk}, the complex-valued coupling from Ring k to Ring j. Naturally, coupling between a ring and a bus waveguide contributes to decay of the ring's energy. Thus, it follows from energy conservation and time reversibility [29,30] that

$$\gamma_j = \gamma_0 + \gamma_{je}, \quad j = 1, 2. \tag{3}$$

Here γ_0 is the rings' intrinsic decay rate. This rate is assumed equal for both rings for simplicity. Interring coupling is assumed to conserve the rings' total energy. Then it follows that κ_{12} and κ_{21} are related as [29,30]

$$\kappa_{12} = \kappa_{21}^*. \tag{4}$$

Thus, for succinctness, we henceforth write κ_{12} as κ and κ_{21} as κ^*.

To induce CAFC on our two-ring system, we modulate the rings' resonance frequencies $\omega_j(t)$ in the following way. First, we let them be separated by a difference $\Delta_0[\Delta_0 = \omega_1(-\infty) - \omega_2(-\infty)]$, sufficiently large in magnitude compared to the interring coupling magnitude $|\kappa|$ to inhibit energy exchange between the rings. While the bare ring frequencies $\omega_j(t)$ remain separated in this way, the optical input (resonant with Ring 1) is launched into the input bus. Then, on a timescale short compared to the TCMT parameters and the ring duration, $\omega_1(t)$ is decreased by $\Delta_0/2$ and $\omega_2(t)$ increased by $\Delta_0/2$ to bring them in resonance with each other. As a result, energy exchange analogous to Rabi oscillation is induced between the rings [38]. This energy exchange is allowed until the energy in Ring 2 reaches its maximum and contains most of the coupled rings' energy. Then the rings' resonance frequencies are restored to their initial values, separated by Δ_0, again on a comparatively short timescale. In this way, the optical pulse, originally at resonance with Ring 1 at frequency $\bar{\omega} + \Delta_0/2$, is now in Ring 2, with frequency $\bar{\omega} - \Delta_0/2$. Thus, a frequency shift of Δ_0 is achieved even when only frequency modulations of $\pm\Delta_0/2$ are applied to each ring.

According to the preceding modulation protocol, we can write $\omega_j(t)$ in the form

$$\omega_j(t) = \bar{\omega} - (-1)^j(\Delta_0/2)[\Theta(t_1 - t) + \Theta(t - t_2)]. \tag{5}$$

In Eq. (5), t_1 and t_2 are the times at which frequency modulation is started and ended, respectively; and $\Theta(x)$, the Heaviside unit-step function. Of course, by substituting Eq. (5) into Eq. (2), we find that $H(t)$ has a form analogous to the right-hand side of Eq. (5), given by

$$H(t) = H_m + (H_0 - H_m)[\Theta(t_1 - t) + \Theta(t - t_2)]. \tag{6}$$

Here H_0 is the value of $H(t)$ before and after ring modulation, and H_m is its value during modulation. Clearly, H_0 is given by Eq. (2) with $\omega_j(t) = \bar{\omega} - (-1)^j(\Delta_0/2)$, and H_m, by Eq. (2) with $\omega_j(t) = \bar{\omega}$.

Given Eqs. (5) and (6), we derive a closed-form expression for the CAFC output $s_{\text{out}}(t)$ in the Supplemental Material [39], under the assumption of large detuning $|\Delta_0|$ compared to the interring coupling $|\kappa|$, the ring decay rates, γ_1 and γ_2, and the input bandwidth. This assumption does not restrict the relevance of the subsequent analysis, because large detuning $|\Delta_0|$ is necessary for efficient CAFC, as we discuss below. This explicit solution for the frequency-shifted $s_{\text{out}}(t)$ is given by

$$s_{\text{out}}(t) = k_{\text{out}}^{\dagger}U(t - t_2, \Delta_0)a(t_2),$$

$$a(t_2) = U(t_2 - t_1, 0)a(t_1),$$

$$a(t_1) = \int_{-\infty}^{\infty} \mathrm{d}t \, U(t_1 - t, \Delta_0)k_{\text{in}}s_{\text{in}}(t). \tag{7}$$

Here $U(t, \Delta)$ is the impulse-response matrix of Eq. (1) for time-independent $H(t)$ with interring detuning Δ. Explicit expressions for the matrix elements of $U(t, \Delta)$ are also given in the Supplemental Material [39].

The proposed scheme for CAFC can be generalized to incorporate N initially detuned, sequentially coupled rings, rather than just two, with N being any integer greater than two. In such a scheme, Ring 1 couples to the input waveguide; Ring N, to the output waveguide; and Ring j ($j = 2, \ldots, N - 1$), to Rings $(j - 1)$ and $(j + 1)$. Ring N is detuned Δ_0 from Ring 1; Ring 2 is detuned by $3\Delta_0/(2N)$ from Ring 1; and Ring j ($j = 1, 2, \ldots N - 1$) is initially detuned by Δ_0/N from Ring $(j - 1)$. In this scheme, light is coupled into Ring 1 from the waveguide. Then Ring 1 is modulated by Δ_0/N and Ring 2 by $-\Delta_0/(2N)$ so they are at resonance with each other and exchange energy. Then Ring 2 is modulated by $\Delta_0/2$ and Ring 3 by $-\Delta_0/2$ and they exchange energy, and so on. Finally, the excited Ring $(N - 1)$ is modulated by $\Delta_0/(2N)$, and Ring N, by $-\Delta_0/N$, until Ring N reaches its maximum energy; and then Ring N is returned to its original frequency and releases its energy into the output waveguide. With this scheme, a net shift of Δ_0 is then achieved, when each ring was modulated by Δ_0/N.

Generalization of the derivation for Eq. (7) to the case of N coupled rings can be done via the same methods of the Supplemental Material [39] for two rings and is straightforward. One then obtains

$$s_{\text{out}}(t) = k^{\text{out}}U_N(t - t_N)a(t_N),$$

$$a(t_{j+1}) = U_j(t_{j+1} - t_j)a(t_j), \quad j = 1, \ldots, N - 1,$$

$$a(t_1) = \int_{-\infty}^{\infty} \mathrm{d}t \, U_0(t_1 - t)k_{\text{in}}s_{\text{in}}(t). \tag{8}$$

Here $U_0(t)$ is the impulse-response matrix before any modulation is applied, and $U_j(t)$, the impulse-response matrix after the Nth modulation is applied. We note that, while the impulse-response matrix in Eq. (7) is 2×2, those in Eq. (8) are $N \times N$, as they describe the time evolution of all N rings.

Though analytical study of the N-ring system is straightforward, its numerical analysis is generally challenging, as it increases the number of parameters with respect to which one must optimize the CAFC process. For this reason, we mostly restrict subsequent analysis to the two-ring system and briefly suggest generalizations to the N-ring system where appropriate.

III. DESCRIPTION OF A SAMPLE CAFC PROCESS

To visualize the temporal dynamics of CAFC, we consider a specific example and numerically evaluate the corresponding temporal dependence of the input power $|s_{out}(t)|^2$, the output power $|s_{out}(t)|^2$, and the ring energies $|a_j(t)|^2$ ($j = 1, 2$).

As in Refs. [28,37], we consider an input $s_{in}(t)$ of the form of a raised-cosine pulse:

$$\begin{aligned}
s_{in}(t) = &\sqrt{2U_s/3T_s}[1 + \cos(2\pi t/T_s)] \\
&\times [\Theta(t + T_s/2) - \Theta(t - T_s/2)] \\
&\times \exp[-i(\bar{\omega} + s\Omega_0^{(r)}/2)t].
\end{aligned} \quad (9)$$

Here T_s is the pulse's duration; U_s, the pulse's total energy; and $\Theta(t)$, the Heaviside unit-step function. To match the resonance frequency of the rings' supermode with most energy in Ring 1, the input carrier frequency is set to $\bar{\omega} + s\Omega_0^{(r)}/2$. Here $s \equiv \text{sgn}(\Delta_0)$ and $\Omega_0^{(r)} \equiv \Re\Omega_0$, where Ω_0 is the ring supermodes' complex-valued frequency splitting in the absence of ring modulation. As discussed in the Supplemental Material [39], Ω_0 is given in terms of the ring parameters by

$$\Omega_0 = \sqrt{(\Delta_0 - i\delta)^2 + 4|\kappa|^2}, \quad \Re\Omega_0 > 0. \quad (10)$$

Here $\delta \equiv (\gamma_1 - \gamma_2)$ is the ring decay rate contrast.

The raised-cosine pulse of Eq. (9) is convenient for our analysis for two reasons. First, it is a symmetric, single-lobe pulse. Hence, it is comparatively robust to dispersive effects for a fixed pulse duration, and it is thus of interest for optical telecommuncations [5,36]. Second, it is nonzero only over a finite time interval, which simplifies the numerical evaluation of the TCMT equations [Eq. (1)] and the optimization of the modulation times t_1 and t_2. As for simple (i.e., not cascaded) AFC in one [28] and two [37] rings, the CAFC of the raised-cosine pulse is mostly governed by the latter's symmetry and single-lobe nature. Thus, the analysis of CAFC of the raised-cosine input applies qualitatively and yields similar results for other symmetric, single-lobe pulse shapes such as Gaussian, super-Gaussian, and hyperbolic secant.

As we show in later sections, the efficiency of CAFC is limited by three distinct normalized timescales. These are the loss per pulse duration, $\gamma_0 T_s$; the interring coupling per pulse duration, $|\kappa|T_s$; and the interring coupling over the interring detuning rate, $|\kappa/\Delta_0|$. The CAFC energy efficiency η increases monotonically as these ratios converge as $\gamma_0 T_s \to 0$, $|\kappa|T_s \to \infty$, and $|\kappa/\Delta_0| \to 0$. Of course, in practice all three

dimensionless ratios have finite, nonzero values. For our sample numerical evaluation of CAFC, we fix the value of $\gamma_0 T_s$ and $|\kappa|T_s$, but sweep the value of $|\kappa/\Delta_0|$. For concreteness, we choose $\gamma_0 T_s = 0$ and $|\kappa|T_s = 10$. Although $\gamma_0 T_s = 0$ is clearly an idealization, we find that the resulting energy-transfer dynamics are representative, i.e., they do not change qualitatively as $\gamma_0 T_s$ increases beyond zero. Furthermore, setting $\gamma_0 = 0$ allows us to illustrate numerically that intrinsic ring loss is not the only physical mechanism limiting the CAFC efficiency, as discussed in Refs. [28,37].

Thus, we solve the TCMT equations, i.e., Eq. (1), numerically for the raised-cosine input $s_{in}(t)$ in Eq. (9), $\gamma_0 = 0$, $|\kappa|T_s = 10$, and various values of $|\Delta_0/\kappa|$, including the limit $|\Delta_0/\kappa| = \infty$. We choose the modulation times, t_1 and t_2, and the bus-ring coupling rates, γ_{1e} and γ_{2e} to approximately optimize the CAFC efficiency, using the schemes explained below in Sec. V. In Fig. 2 we plot the resulting instantaneous energies, $|a_1(t)|^2$ and $|a_2(t)|^2$, and instantaneous powers, $|s_{in}(t)|^2$ and $|s_{out}(t)|^2$.

We first analyze the time dependence of the instantaneous powers and energies in Fig. 2 for $|\Delta_0/\kappa| = \infty$. Then we analyze the changes these quantities undergo as $|\Delta_0/\kappa|$ becomes finite and progressively decreases. For $|\Delta_0/\kappa| = \infty$, from the start of the pulse at $t = -T_s/2$ and until the start of ring modulation at $t = t_1$, $|a_1(t)|^2$ increases monotonically while $|a_2(t)|^2$ stays at zero. This is because, for $|\Delta_0/\kappa| = \infty$, the energy transferred from Ring 1 to Ring 2 cannot accumulate before the field amplitude in the rings grow out of phase with each other. Thus, the energy in Ring 2 is effectively isolated from Ring 1, and the power injected through the input bus accumulates in Ring 1.

From $t = t_1$ to $t = t_2$, ring modulation is applied so that the interring detuning Δ vanishes. Thus, the input $s_{in}(t)$ is no longer at resonance with a ring supermode. Consequently, loading of the input $s_{in}(t)$ into Ring 1 becomes inhibited, but interring energy exchange is no longer so. Hence $|a_1(t)|^2$ decreases while $|a_2(t)|^2$ increases. The time dependence of the ring energies in this time interval is approximately sinusoidal, in analogy to Rabi oscillation [29,38]. Albeit the total energy in both rings decays exponentially with rate $(\gamma_1 + \gamma_2)$, which we show below must be of the order of the input bandwidth $\sim T_s^{-1}$ for efficient, bandwidth-preserving CAFC. Even if the rings' intrinsic decay rate γ_0 vanishes, the total decay rate $(\gamma_1 + \gamma_2) = (\gamma_{1e} + \gamma_{2e})$ is nonzero because we need nonvanishing γ_{1e} and γ_{2e} to couple the optical pulse from the input bus into Ring 1 and from Ring 2 into the output bus.

Ring modulation stops at $t = t_2$. The stopping time t_2 is chosen so that the energy transferred from Ring 1 to Ring 2 is approximately maximum. So to zeroth order in $\gamma_1/|\kappa|$ and $\gamma_2/|\kappa|$, t_2 is set so that $t_2 - t_1 = \pi/(2|\kappa|)$. From this statement and from the last paragraph, it follows that efficient interring energy transfer requires $(\gamma_1 + \gamma_2)(t_2 - t_1) \sim (|\kappa|T_s)^{-1} \ll 1$. Otherwise, a significant fraction of the rings' energy is leaked into the bus wave guides during interring transfer. For the considered value of $|\kappa|T_s$, this energy leakage causes the maximum $|a_2(t_1)|^2$ in Fig. 2 to be appreciably smaller than the maximum for $|a_1(t_1)|^2$ at $|\Delta_0/\kappa| = \infty$. For $t > t_2$, interring energy exchange is again inhibited by the large ratio $|\Delta_0/\kappa|$, so the energy in Ring 2 is isolated from Ring 1. From Ring 2, the energy leaks continuously into the output bus with rate γ_{2e},
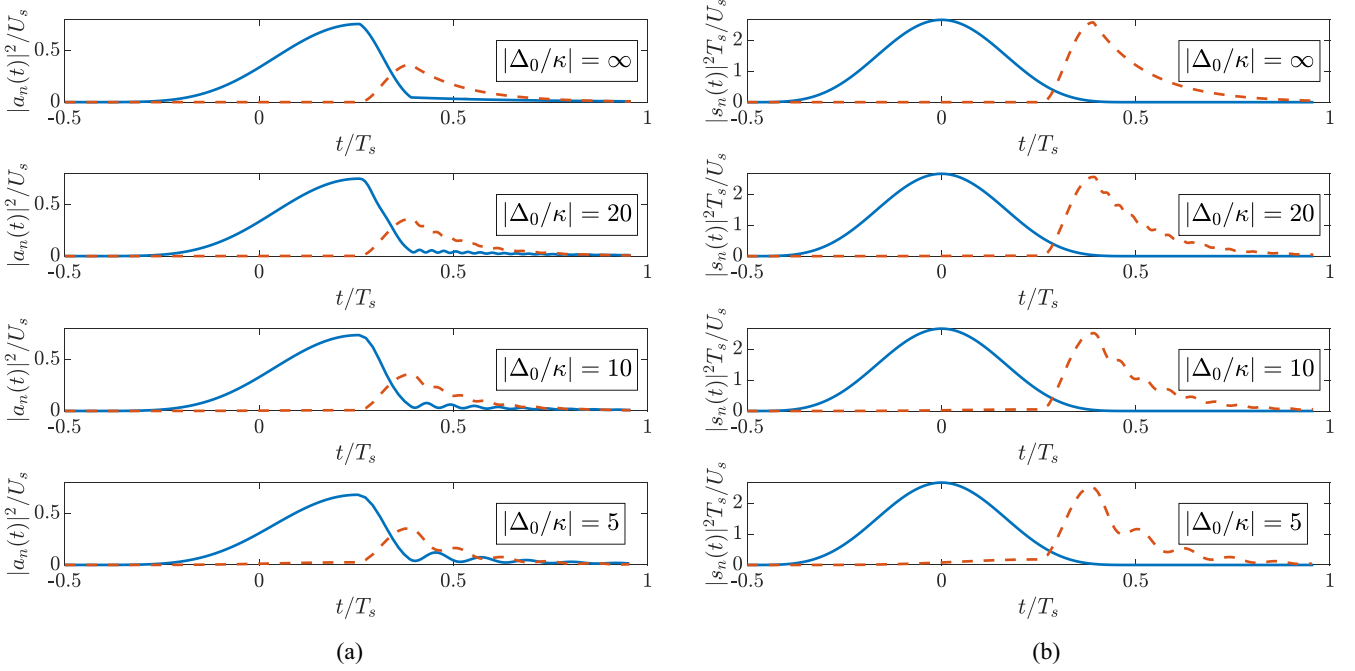
FIG. 2. Plots of the instantaneous ring energies and the instantaneous input and output powers as functions of time t for a raised-cosine input, $\gamma_0 = 0$, $|\kappa|T_s = 10$, and various values of $|\Delta_0/\kappa|$. U_s is the input energy and T_s, the input's duration: (a) ring energies, $|a_1(t)|^2$ (solid blue) and $|a_2(t)|^2$ (dashed orange), as functions of time t; (b) input and output powers, $|s_{\text{in}}(t)|^2$ (solid blue) and $|s_{\text{out}}(t)|^2$ (dashed orange), as functions of time t.

and its amplitude oscillates at frequency ω_2 (or $\bar{\omega} - s\Omega_0^{(r)}/2$, for finite $|\Delta_0/\kappa|$).

As a consequence of Eq. (1), $|s_{\text{out}}(t)|^2$ is proportional to $|a_2(t)|^2$. However, as we noted earlier, not all of the energy in the output $s_{\text{out}}(t)$ oscillates at the target output frequency ω_2 (or $\bar{\omega} - s\Omega_0/2$, for finite $|\Delta_0/\kappa|$). Only the energy in $s_{\text{out}}(t)$ for $t > t_2$ oscillates at this frequency. Therefore, only the segment of $s_{\text{in}}(t)$ for $t > t_2$ [mathematically given by $s_{\text{out}}(t)\Theta(t - t_2)$] corresponds to the frequency-shifted output. Thus, in the limit of $|\Delta_0/\kappa| \to \infty$, the frequency-shifted output equals exactly an exponentially decaying tail starting suddenly at $t = t_2$, decaying in power with rate $2\gamma_2$, and oscillating in amplitude at the target frequency $\omega_2 = \omega_1 - \Delta_0$. In the limit of large $|\Delta_0/\kappa|$, the total energy in this frequency-shifted output is $(\gamma_{2e}/\gamma_2)|a_2(t_2)|^2$. We choose $\gamma_{2e} = 1/(2T_{\text{RMS}})$ so that the input and frequency-shifted output power signals have the same root-mean-square duration in this limit. This choice of γ_{2e} and its implication on the CAFC efficiency are discussed in detail in the Supplemental Material [39].

As $|\Delta_0/\kappa|$ becomes finite, several new effects appear in the energy and power dynamics of CAFC. First, the maximum energy $|a_1(t_1)|^2$ loaded from the bus into Ring 1 decreases, as Ring 1 is continuously leaking energy into Ring 2. Second, the splitting in the rings' supermode resonance frequencies changes from Δ_0 to $\Omega_0^{(r)}$, as discussed for Eq. (9). Third, the decay rates of the supermodes also change. They are modified from their bare values of γ_j ($j = 1, 2$) to new values $\tilde{\gamma}_j$, defined as

$$\tilde{\gamma}_j = \bar{\gamma} + (-1)^j s\Omega_0^{(i)}/2. \tag{11}$$

Here $\bar{\gamma} = (\gamma_1 + \gamma_2)/2$ is the ring-averaged decay rate, and $\Omega_0^{(i)} \equiv \Im\Omega_0$. As a consequence of this alteration of the effective decay rates $\tilde{\gamma}_j$, both the optimal time t_1 to start modulation and the optimal coupling between bus and Ring 1 γ_{1e} are correspondingly modified. This modification of the optimal values for t_1 and γ_{1e} is studied below in Sec. V.

Because $|a_1(t_1)|^2$ decreases, the maximum energy in Ring 2 at the end of modulation, $|a_2(t_2)|^2$, diminishes proportionally. Beyond that, the Rabi oscillation in ring energy from $t = t_1$ to $t = t_2$, remains unchanged, as it does not depend on $|\Delta_0|$. This is because we keep the modulation time $(t_2 - t_1)$ fixed for simplicity. In addition to the Rabi oscillation of the rings' energy, for finite $|\Delta_0/\kappa|$ energy from $s_{\text{in}}(t)$ can couple into the rings during ring modulation at $t \in [t_1, t_2]$. However, this effect is negligible as long as $|\Delta_0/\kappa|$ is large enough that the input bandwidth, $\sim T_s^{-1}$, is small compared to the shift in the supermode's resonance frequencies due to ring modulation, $\sim(|\Delta_0| - |\kappa|)$. This is the case for the TCMT parameters used for Fig. 2.

As $|\Delta_0/\kappa|$ becomes finite, the energy in Ring 2, $|a_2(t)|^2$, for $t > t_2$ no longer merely decays exponentially at the bare-ring rate γ_2. Due to interference between the supermodes, $|a_2(t)|^2$ for $t > t_2$ becomes the sum of three terms: two decaying exponentially, one at rate $2\tilde{\gamma}_1$ and the other at rate $2\tilde{\gamma}_2$, and one oscillating with angular frequency $\Omega_0^{(r)}$ and with envelope decaying as $2\bar{\gamma} = (\gamma_1 + \gamma_2)$. For large $|\Delta_0/\kappa|$, the term decaying as $\tilde{\gamma}_2$ dominates. But as $|\Delta_0/\kappa|$ decreases, the other two terms become appreciable. This can be seen in Fig. 2, where the oscillating term causes a beat in Ring 2's energy, $|a_2(t_2)|^2$, which progressively increases in amplitude and decreases in frequency as $|\Delta_0/\kappa|$ decreases. The term decaying as $\tilde{\gamma}_1$ is not discernible in Fig. 2 as, in this case,

$\tilde{\gamma}_1 \approx \tilde{\gamma}_2$. In theory, $|a_2(t)|^2$ for $t > t_2$ is also altered by the energy in $s_{\rm in}(t)$ for $t > t_2$. However, the large detuning $|\Delta_0|$ compared to the input bandwidth T_s^{-1} again causes this effect to be negligible.

IV. INNER-PRODUCT ANALYSIS OF THE CAFC EFFICIENCY

To analyze the efficiency of CAFC, it is useful to identify the input $s_{\rm in}(t)$ and the frequency-shifted output $s_{\rm out}(t)$ as vectors in the vector space of finite-energy pulses (mathematically, the Hilbert space of square integrable functions of time, L^2) as in Ref. [37]. Using Dirac notation, let $|f(t)\rangle$ and $|g(t)\rangle$ be vectors in this Hilbert space corresponding to the square-integrable functions functions of time t, $f(t)$ and $g(t)$, respectively. We define the inner product between these vectors as

$$\langle f(t)|g(t)\rangle \equiv \int_{-\infty}^{\infty} dt \, f^*(t) g(t). \tag{12}$$

Employing this Dirac notation, we rewrite Eq. (7) in the more abstract form

$$\begin{aligned} |s_{\rm out}(t)\rangle &= \hat{T}_{\rm out} a(t_2), \\ a(t_2) &= U(t_2 - t_1, 0) a(t_1), \\ a(t_1) &= \hat{T}_{\rm in} |s_{\rm in}(t)\rangle. \end{aligned} \tag{13}$$

In Eqs. (13), $\hat{T}_{\rm out}$ is a linear map from the vector space of two-dimensional, complex-valued vectors, $\mathbb{C}^2$, to L^2. Conversely, $\hat{T}_{\rm in}$ is a linear map from L^2 to $\mathbb{C}^2$. Let $u_{jk}(t, \Delta)$ be the matrix element of $U(t, \Delta)$ from Eqs. (7) and (13) in its jth row and kth column. Then we can write explicit expressions for the $\hat{T}_{\rm in}$ and $\hat{T}_{\rm out}$ maps as

$$\begin{aligned} \hat{T}_{\rm out} &= \sqrt{2\gamma_{2e}}(|u_{21}(t - t_2, \Delta_0)\rangle \; |u_{22}(t - t_2, \Delta_0)\rangle), \\ \hat{T}_{\rm in} &= \sqrt{2\gamma_{1e}} \begin{pmatrix} \langle u_{11}^*(t - t_1, \Delta_0)| \\ \langle u_{21}^*(t - t_1, \Delta_0)| \end{pmatrix}. \end{aligned} \tag{14}$$

The conjugation of the impulse response functions $u_{j1}(t - t_1, \Delta_0)$ ($j = 1, 2$) in Eq. (14) results from the definition of the inner product, Eq. (12). As implied by their subindices, $\hat{T}_{\rm in}$ describes the loading of the input optical pulse into the coupled rings, and $\hat{T}_{\rm out}$, the unloading of the ring energy into the frequency-shifted output. From Eq. (14), it follows that the net action of CAFC is that of a linear operator $\hat{T}$ in L^2, transforming $|s_{\rm in}(t)\rangle$ into $|s_{\rm out}(t)\rangle$. Furthermore, this operator is expressible as

$$\hat{T} = \hat{T}_{\rm out} U(t_2 - t_1, 0) \hat{T}_{\rm in}. \tag{15}$$

Equations (14) and (15) suggest that $\hat{T}_{\rm out}$, $\hat{T}_{\rm in}$, and $\hat{T}$ are maps of rank 2, i.e., that their image is a two-dimensional vector space. In practice, this is inaccurate because, for CAFC, we consider only inputs $|s_{\rm in}(t)\rangle$ nearly resonant with Ring 1's original frequency ($\omega_0 + \Delta_0/2$), and outputs $|s_{\rm out}(t)\rangle$ resonant with Ring 2;s final frequency ($\omega_0 - \Delta_0/2$), rather than over the complete frequency spectrum. Thus, the co-image of $\hat{T}_{\rm in}$ and the image of $\hat{T}_{\rm out}$ are practically restricted, which might reduce the rank of $\hat{T}_{\rm in}$, $\hat{T}_{\rm out}$ and $\hat{T}$ and impact the resulting efficiency of CAFC. To incorporate this restriction into our analysis, we introduce effective "filtered" maps $\hat{T}_{{\rm in}, F}$, $\hat{T}_{{\rm out}, F}$,

and $\hat{T}_F$. Explicitly, the filtered loading map, $\hat{T}_{{\rm in}, F}$, is defined so that it models the effect of $\hat{T}_{\rm in}$ only over the vector space of inputs $|s_{\rm in}(t)\rangle$ nearly resonant to Ring 1 before modulation. On the other hand, the filtered unloading map, $\hat{T}_{{\rm out}, F}$, is the restriction of $\hat{T}_{\rm out}$ to the preimage of outputs $|s_{\rm out}(t)\rangle$ nearly resonant to Ring 2 after modulation. Finally, $\hat{T}_F$ is defined, in analogy to Eq. (15), as

$$\hat{T}_F = \hat{T}_{{\rm out}, F} U(t_2 - t_1, 0) \hat{T}_{{\rm in}, F}. \tag{16}$$

As given in Eq. (16), $\hat{T}_F$ describes the output of $\hat{T}$ nearly resonant to Ring 2, restricted over inputs $|s_{\rm in}(t)\rangle$ nearly resonant to Ring 1.

For subsequent analysis, we formulate abstract expressions for the filtered maps. To do so, we note from the Supplemental Material [39] that, before and after modulation, the ring supermodes oscillate at the frequencies $\bar{\omega} \pm \Omega_0^{(r)}/2$. Thus, we write

$$\begin{aligned} \hat{T}_{{\rm in}, F} &= \hat{T}_{\rm in} \hat{F}(\bar{\omega} + s\Omega_0^{(r)}/2), \\ \hat{T}_{{\rm out}, F} &= \hat{F}(\bar{\omega} - s\Omega_0^{(r)}/2) \hat{T}_{\rm out}. \end{aligned} \tag{17}$$

Here $\hat{F}(\omega)$ is an ideal bandpass-filter operator, which retains only pulses near-resonant with ω. As in Sec. III, $s = {\rm sgn}(\Delta_0)$. Of course, the ideal bandpass-filter $\hat{F}(\omega)$ must have a given bandwidth. We assume that this bandwidth is large compared to typical bandwidths of the considered inputs $|s_{\rm in}(t)\rangle$ and outputs $|s_{\rm out}(t)\rangle$, albeit small compared to the ring detuning Δ_0 and leave it unspecified.

We take the ideal filter operator $\hat{F}(\omega)$ as self-adjoint. Thus, we may evaluate the right-hand sides of (17) by applying $\hat{F}(\omega)$ to the bras $\langle u_{j1}^*(t - t_1, \Delta_0)|$ and the kets $|u_{2j}(t - t_2, \Delta_0)\rangle$ ($j = 1, 2$) in Eq. (14). We do so by retaining only the terms in the matrix elements $u_{nm}(t, \Delta_0)$ oscillating at the frequency specified by the filtering operator $\hat{F}(\omega)$, either $(\bar{\omega} + s\Omega_0^{(r)}/2)$ or $(\bar{\omega} - s\Omega_0^{(r)}/2)$. In this way, we obtain the explicit expressions

$$\begin{aligned} \hat{T}_{{\rm in}, F} &= \sqrt{\frac{\gamma_{1e}}{\tilde{\gamma}_1}} \begin{pmatrix} [1 + (|\Delta_0| - is\delta)/\Omega_0]/2 \\ s\kappa_{21}/\Omega_0 \end{pmatrix} \langle n_{\rm in}|, \\ \hat{T}_{{\rm out}, F} &= \sqrt{\frac{\gamma_{2e}}{\tilde{\gamma}_2}} |n_{\rm out}\rangle (-s\kappa_{21}/\Omega_0 [1 + (|\Delta_0| - is\delta)/\Omega_0]/2). \end{aligned} \tag{18}$$

In Eq. (18), $|n_{\rm in}\rangle$ and $\langle n_{\rm out}|$ are the ket and bra corresponding, respectively, to the normalized pulses

$$\begin{aligned} n_{\rm in}(t) &= \sqrt{2\tilde{\gamma}_1} \Theta(t_1 - t) \exp[-(t_1 - t)(\bar{\gamma} - i\bar{\omega} - is\Omega_0^*/2)], \\ n_{\rm out}(t) &= \sqrt{2\tilde{\gamma}_2} \Theta(t - t_2) \exp[-(t - t_2)(\bar{\gamma} + i\bar{\omega} - is\Omega_0/2)]. \end{aligned} \tag{19}$$

Again, $\Theta(t)$ is the Heaviside function, and $\tilde{\gamma}_j$, the modified decay rates of Eq. (11). The bra $\langle n_{\rm in}|$ and the ket $|n_{\rm out}\rangle$ in Eq. (18) are normalized so that $\langle n_{\rm in}|n_{\rm in}\rangle = \langle n_{\rm out}|n_{\rm out}\rangle = 1$. From Eqs. (16) and (18), it is clear that the filtered maps $\hat{T}_{{\rm in}, F}$, $\hat{T}_{{\rm out}, F}$, and $\hat{T}_F$ are of rank 1. This is in contrast to the unfiltered maps $\hat{T}_{\rm in}$, $\hat{T}_{\rm out}$, and $\hat{T}$ in Eqs. (14) and (15), which are of rank 2. As we discuss next, consideration of this rank reduction is key to analyze CAFC efficiency's upper bounds and its dependence on the input pulse $s_{\rm in}(t)$.

Leveraging Eqs. (16) and (18), it is now straightforward to write an explicit expression for the energy efficiency η of CAFC. Since the CAFC output is given by $\hat{T}_F |s_{\text{in}}(t)\rangle$, we substitute Eqs. (16) and (18) to obtain

$$\eta = \frac{\langle s_{\text{in}}(t)|\hat{T}_F^{\dagger}\hat{T}_F|s_{\text{in}}(t)\rangle}{\langle s_{\text{in}}(t)|s_{\text{in}}(t)\rangle} = \frac{\gamma_{1e}\gamma_{2e}}{\tilde{\gamma}_1\tilde{\gamma}_2}|V|^2 \frac{|\langle n_{\text{in}}|s_{\text{in}}(t)\rangle|^2}{\langle s_{\text{in}}(t)|s_{\text{in}}(t)\rangle}. \quad (20)$$

Here $\dagger$ stands for the adjoint operation, and V, for the matrix product

$$V = (-s\kappa_{21}/\Omega_0 [1 + (|\Delta_0| - is\delta)/\Omega_0]/2)$$
$$\times\ U(t_2 - t_1, 0)\begin{pmatrix} [1 + (|\Delta_0| - is\delta)/\Omega_0]/2 \\ s\kappa_{21}/\Omega_0 \end{pmatrix}. \quad (21)$$

Of course, the magnitude of the inner product $\langle n_{\text{in}}|s_{\text{in}}(t)\rangle$ is bounded by the Schwarz inequality [28,51] as $|\langle n_{\text{in}}|s_{\text{in}}(t)\rangle|^2 \leqslant \langle n_{\text{in}}|n_{\text{in}}\rangle\langle s_{\text{in}}(t)|s_{\text{in}}(t)\rangle = \langle s_{\text{in}}(t)|s_{\text{in}}(t)\rangle$. Hence, the CAFC efficiency η is bounded from above as

$$\eta \leqslant \frac{\gamma_{1e}\gamma_{2e}}{\tilde{\gamma}_1\tilde{\gamma}_2}|V|^2. \quad (22)$$

Furthermore, this bound is tight; as a well-known corollary of the Schwarz inequality is that it becomes an equality if and only if the two vectors considered are linearly dependent [51]. Thus, Eq. (22) becomes an equality if and only if $|s_{\text{in}}(t)\rangle$ is proportional to $|n_{\text{in}}\rangle$. Additionally, increasing the projection of $|s_{\text{in}}(t)\rangle$ into $|n_{\text{in}}\rangle$ increases the ratio $|\langle n_{\text{in}}|s_{\text{in}}(t)\rangle|^2/\langle s_{\text{in}}(t)|s_{\text{in}}(t)\rangle$, and thus increases the efficiency η, providing the remaining factors on the right-hand side of Eq. (20) remain fixed.

Generalization of the results of this section to the N-ring system is straightforward. The row vector of kets and the column vector of bras in Eq. (18) for $\hat{T}_{\text{out}}$ now have entries $|u_{Nj}^{(N)}(t - t_N)\rangle$ and $\langle u_{j1}^{(0)*}(t - t_1)|$, respectively. Here $u_{kl}^{(j)}(t)$ is the kl entry of the impulse-response matrix $U_j(t)$, as defined in Eq. (8). Equations (15), (16), and (21), the matrix $U(t_2 - t_1, 0)$ is replaced by the matrix product

$$U(t_2 - t_1, 0) \rightarrow \prod_{j=1}^{N-1} U_j(t_{j+1} - t_j). \quad (23)$$

In the right-hand side of Eq. (23), the matrices $U_j(t_{j+1} - t_j)$ are multiplied in descending order for their index j.

In the N-ring system, the rings' supermodes no longer oscillate at the complex frequencies $\bar{\omega} - i\bar{\gamma} \pm \Omega_0/2$ before and after modulation. Rather, they oscillate at the complex frequencies is_j ($j = 1, \ldots, N$). These s_j are the poles of the resolvent $(sI_N + iH_0)^{-1}$, where I_N is the $N \times N$ identity matrix, and H_0, as in Eq. (6), is the frequency-coefficient matrix $H(t)$ before and after all ring modulations. Consequently, the filtering frequencies $\bar{\omega} \pm \Omega_0^{(r)}/2$ in Eq. (17) must be changed to $-\Im s_1$ and $-\Im s_N$, respectively. Here is_j is the complex supermode frequency with $-\Im s_j$ closest to the bare resonance frequency of the jth Ring. Additionally, the input and output normalized pulses $n_{\text{in}}(t)$ and $n_{\text{out}}(t)$ in Eq. (19) retain the same form, with their central frequencies replaced by $-\Im s_1$ and $-\Im s_N$, and their decay rates by $-\Re s_1$ and $-\Re s_N$, respectively. Of course, the expressions for column and row vectors in Eq. (14) and (21) become altered for the N-ring system, and must be reevaluated for each value of N.

Limit of large interring detuning

To aid the numerical optimization of the CAFC efficiency η and to develop an intuition of its behavior, it is useful to consider η in the limit of large interring detuning $|\Delta_0|$ compared to the other time rates governing the CAFC process. Expressly, this limit corresponds to that of $|\Delta_0|$ large compared to the interring coupling $|\kappa|$, the ring decay rates γ_j ($j = 1, 2$), and the input pulse's bandwidth. Let us define η_0 as the CAFC efficiency in this limit, i.e., $\eta_0 = \lim_{|\Delta_0| \to \infty} \eta$. From Eq. (20) for η, we find that η_0 can be factored as

$$\eta_0 = \eta_{01}\eta_{12}\eta_{23}. \quad (24)$$

Here the factors $\eta_{j,j+1}$ ($j = 0, 1, 2$) on the right-hand side of Eq. (24) can be interpreted as the efficiencies of the subprocesses composing CAFC. η_{01} is the efficiency of loading the input pulse from the input bus waveguide into Ring 1; η_{12}, the efficiency of transferring the energy from Ring 1 to Ring 2; and η_{23}, the efficiency of unloading the energy from Ring 2 into the output bus waveguide. The expressions for these partial efficiencies are

$$\eta_{01} = \left(\frac{\gamma_{1e}}{\gamma_1}\right)\frac{|\langle n_{\text{in}}|s_{\text{in}}(t)\rangle|^2}{\langle s_{\text{in}}(t)|s_{\text{in}}(t)\rangle},$$
$$\eta_{12} = |u_{21}(t_2 - t_1, 0)|^2,$$
$$\eta_{23} = \gamma_{2e}/\gamma_2. \quad (25)$$

Clearly, the expressions in Eq. (25) agree with the previously described interpretations.

Let us briefly discuss the partial efficiencies η_{01} and η_{23}. In the limit $|\Delta_0| \to \infty$, the normalized input vector $|n_{\text{in}}\rangle$, given by Eq. (19), oscillates at frequency ω_1 and grows at a rate of γ_1. Thus, as expected, η_{01} equals the efficiency of loading the input $s_{\text{in}}(t)$ into Ring 1 in the absence of Ring 2 and the output bus [28]. Similarly, the expression for η_{23} in Eq. (25) is identical to the efficiency of unloading the energy in Ring 2 into the bus waveguide in the absence of the input bus and Ring 1 [28].

Just as discussed for Eq. (22), η_{01} in Eq. (25) is bounded by the Schwarz inequality as $\eta_{01} \leqslant \gamma_{1e}/\gamma_1$. Furthermore, from the Schwarz inequality's corollary, η_{01} increases as the projection of $|s_{\text{in}}(t)\rangle$ into $|n_{\text{in}}\rangle$ increments, if γ_{1e}/γ_1 remains constant. Finally, the maximum $\eta = \gamma_{1e}/\gamma_1$ can be attained if and only if $|s_{\text{in}}(t)\rangle$ is proportional to $|n_{\text{in}}\rangle$.

Though it is difficult to obtain an explicit form for η for CAFC in the N-ring ($N > 2$) system for finite Δ_0, the intuitive results of this subsection suggest it takes a simple form in the limit of infinite $|\Delta_0|$. Given the intuitive forms η_0 in Eq. (24) and of $\eta_{j,j+1}$ in Eq. (25), and the generalization rule Eq. (23), we surmise that, for the N-ring system, η_0 takes the form

$$\eta_0 = \prod_{j=0}^{N} \eta_{j,j+1}. \quad (26)$$

As in the two-ring system, $\eta_{j,j+1}$ ($j = 0, \ldots, N$) are the partial efficiencies of the subprocesses constituting CAFC in the limit $|\Delta_0| \to \infty$. Just as in the two-ring system, η_{01} is the efficiency of loading the input from the input bus into Ring 1, and $\eta_{N,N+1}$, the efficiency of unloading the energy from Ring N into the output bus. These are still given by Eq. (25) for

η_{01} and η_{23}, respectively. For $j \neq 0, N$, $\eta_{j,j+1}$ is the efficiency of transferring energy from Ring j to Ring $(j+1)$. As a consequence of Eq. (23), this is given by

$$\eta_{j,j+1} = \lim_{|\Delta_0| \to \infty} \left| u_{j+1,j}^{(j)}(t_{j+1} - t_j) \right|^2, \quad j \neq 0, N. \quad (27)$$

As described above Eq. (23), $u_{j+1,j}^{(j)}(t)$ are off-diagonal entries of the impulse-response matrix $U_j(t)$.

V. OPTIMIZATION OF THE CAFC TIMESCALES

As is clear from Secs. III and IV, the two-ring CAFC process and its efficiency depend on the relation among various timescales and time rates. These are the pulse duration T_s, the initial t_1 and final t_2 times of modulation, the interring detuning Δ_0, the interring coupling κ, the intrinsic decay rate γ_0, the coupling rate γ_{1e} between the input bus and Ring 2, and the coupling rate γ_{2e} between Ring 2 and the output bus. In this section we describe our scheme for practical numerical optimization of the CAFC efficiency with respect to these variables. For concreteness, we suppose the input pulse is a simple, symmetric, single-lobe pulse as in Sec. III.

First, we discuss CAFC efficiency optimization with respect to the pulse duration T_s. In practice, the input pulse is usually fixed. Hence T_s is often not a free parameter to optimize the CAFC efficiency. For completeness, though, we briefly consider optimization of CAFC with respect to T_s. We see in Eq. (20) that T_s appears only in the expression for the CAFC efficiency η through the inner product $\langle n_{\text{in}} | s_{\text{in}}(t) \rangle$. Thus, if all other TCMT parameters remain constant, optimal T_s is that which maximizes $|\langle n_{\text{in}} | s_{\text{in}}(t) \rangle|$. From Eq. (19), this implies that T_s must be of the order of the supermode decay rate $\tilde{\gamma}_1 \sim \gamma_1$. Furthermore, the derivation of the solution of Eqs. (1) in the Supplemental Material [39] assumes that the bandwidth of $s_{\text{in}}(t)$ is small compared to the modulation-induced change in the rings' supermode resonant frequency, which is of the order of $(|\Delta_0| - |\kappa|)$. This requirement is equivalent to the condition $(|\Delta_0| - |\kappa|)T_s \gg 1$. This condition is satisfied if $|\Delta_0| \gg |\kappa|$ and $|\kappa|T_s \gg 1$, which are necessary for efficient CAFC, as discussed in Sec. III and below in this section. Nonetheless, as discussed below in this section and Sec. VI, efficient CAFC under our scheme requires simultaneously $\gamma_0 T_s \ll 1$ and $|\kappa|T_s \gg 1$. The first condition arises because efficient CAFC requires both $\gamma_{1e} \gg \gamma_0$ and $\gamma_{1e} \sim T_s^{-1}$, as explained below in this section, which occurs only if $\gamma_0 T_s \ll 1$. Similarly, the second condition emerges because efficient CAFC requires $\gamma_{1e} \ll |\kappa|$ and $\gamma_{1e} \sim T_s^{-1}$, again explained below, which occurs only if $|\kappa|T_s \gg 1$.

Second, we consider CAFC optimization with respect to the modulation start time t_1. From Eqs. (19) and (20), t_1 appears only in the expression for η through the bra vector $\langle n_{\text{in}} |$ in the inner product $\langle n_{\text{in}} | s_{\text{in}}(t) \rangle$. Specifically, t_1 is the time at which the normalized, truncated, increasing exponential $n_{\text{in}}(t)$ is terminated. Thus, the value of t_1 which optimizes η is the one which shifts $|n_{\text{in}}\rangle$ so that it achieves the largest overlap with $|s_{\text{in}}(t)\rangle$. For a large detuning ratio $|\Delta_0/\kappa|$, the CAFC optimization with respect to t_1 can be interpreted as an optimization of the loading of the input pulse into one of the rings' supermodes at time t_1.

Third, we examine CAFC optimization with respect to the modulation end time t_2. For a high modulation ratio $|\Delta_0/\kappa|$ and small input bandwidth $|\kappa| \gg T_s^{-1}$, coupling of $s_{\text{in}}(t)$ into the rings is inhibited during ring modulation, from $t = t_1$ to $t = t_2$. Thus, the only effect of varying t_2 is to modify the duration $(t_2 - t_1)$ of Rabi oscillation of the rings' energies. This is seen from Eqs. (20) and (21). Thus, to optimize the CAFC efficiency η with respect to t_2, we choose the t_2 which maximizes the modulus of V in Eq. (21). Nonetheless, direct maximization of $|V|^2$ for finite Δ_0 is a challenging problem, requiring numerical solution for each value of $|\Delta_0/\kappa|$. To simplify the problem, we note, as in Sec. IV A, that $\lim_{\Delta_0 \to \infty} V = u_{21}(t_2 - t_1, 0)$. Furthermore, maximization of $\eta_{12} = |u_{21}(t_2 - t_1, 0)|^2$ with respect to t_2 can be performed analytically for arbitrary values of the other TCMT parameters. This analytical optimization is discussed in the Supplemental Material [39]. Thus, for simplicity of numerical implementation, we set t_2 to the value which maximizes η_{12}, and thus η in the limit of high $|\Delta_0|$. Of course, this value of t_2 also approximately maximizes $|V|^2$ (and thus the exact CAFC efficiency η) for large $|\Delta_0/\kappa|$, which itself is necessary for efficient CAFC.

Fourth, we discuss the effect of the pre- and post-modulation interring detuning Δ_0 on the CAFC efficiency. Mathematically, changing Δ_0 changes the pre- and postmodulation rings' supermodes and their complex-valued frequency splitting Ω_0. Consequently, this changes the supermodes' modified decay rates $\tilde{\gamma}_j$ in Eq. (11), which modifies the input and output functions $n_{\text{in}}(t)$ and $n_{\text{out}}(t)$ in Eq. (19). Increasing $|\Delta_0|$ modifies the supermodes by causing them to concentrate each on one of the two rings. This energy concentration reduces the interring energy leakage before and after ring modulation, and thus increases the CAFC efficiency. In particular, to inhibit interring energy exchange before and after modulation, we must have $|\Delta_0/\kappa| \gg 1$.

Fifth, we consider the effect of interring coupling κ. Before and after ring modulation, we require $|\kappa|$ to be small compared to $|\Delta_0|$ to inhibit interring energy leakage, as discussed above. During ring modulation, we require $|\kappa|$ to be large compared to the ring-averaged decay rate $\bar{\gamma}$ so that the energy in Ring 1 can be transferred to Ring 2 before the rings' total energy dissipates noticeably. Combining these two criteria, we deduce that there exists an value of $|\kappa|$ that optimizes η, satisfying $\bar{\gamma} \ll |\kappa| \ll |\Delta_0|$. Exact determination of this optimal $|\kappa|$ is a formidable numerical problem. In Sec. VII we present an approximate numerical scheme to estimate this optimal $|\kappa|$.

Sixth, we examine the effect of the intrinsic decay rate γ_0 on the CAFC efficiency. Physically, the effect of nonzero γ_0 is to introduce energy loss at all stages of CAFC. Thus, the CAFC efficiency is maximized with respect to γ_0 in the ideal case of $\gamma_0 = 0$. More specifically, efficient CAFC requires the intrinsic photon lifetime $(2\gamma_0)^{-1}$ large compared to all other timescales of CAFC. Among the remaining timescales, we show below that efficient CAFC requires T_s, $(2\gamma_{1e})^{-1}$, and $(2\gamma_{2e})^{-1}$ to be largest, with these three all being of similar order of magnitude. Thus, a concrete criterion for small intrinsic loss is $\gamma_0 T_s \ll 1$. In particular, $\gamma_0 T_s \sim \gamma_0/\gamma_{1e} \ll 1$ directly implies low intrinsic loss upon coupling of the input into Ring 1 before modulation. Similarly, $\gamma_0 T_s \sim \gamma_0/\gamma_{2e} \ll 1$ implies low intrinsic loss upon coupling the frequency-shifted output out of Ring 2 after modulation.

Seventh, we analyze the net effect on the CAFC efficiency η of the coupling rate γ_{1e} between the input bus and Ring 1. From Eq. (20), η depends on γ_{1e} through three of its factors: $(\gamma_{1e}/\tilde{\gamma}_1)$, $|\langle n_{\text{in}}|s_{\text{in}}(t)\rangle|^2$, and $|V|^2$. In the limit of large $|\Delta_0|$, $(\gamma_{1e}/\tilde{\gamma}_1)$ converges to γ_{1e}/γ_1. So for large $|\Delta_0|$, the ratio $(\gamma_{1e}/\tilde{\gamma}_1)$ increases monotonically with γ_{1e}. In particular, $(\gamma_1/\tilde{\gamma}_1)$ becomes near unity when $\gamma_{1e} \gg \gamma_0$ for large $|\Delta_0|$. On the other hand, the magnitude of the inner product $\langle n_{\text{in}}|s_{\text{in}}(t)\rangle$ is optimized with respect to γ_{1e} when the duration $\tilde{\gamma}_1$ of $n_{\text{in}}(t)$ [in Eq. (19)] is of the order of the input bandwidth $\sim T_s^{-1}$. Finally, in the limit of large $|\Delta_0|$, V converges to $u_{21}(t_2 - t_1, 0)$. Consequently, large $|V|^2 \approx |u_{21}(t_2 - t_1, 0)|^2$ requires γ_{1e} small compared to $|\kappa|$ for large $|\Delta_0|$. Balancing all of these dependences to obtain the value of γ_{1e} which optimizes η is evidently a challenging numerical problem which also depends on the particular value of $|\Delta_0|$. To make the problem numerically amenable, we assume $|\Delta_0|$ large enough so we can optimize the factorized η of Sec. IV A instead of the general η to good accuracy.

To this approximation, we need only balance the dependences on γ_{1e} of the partial efficiencies η_{01} and η_{12} from Eq. (25). From Sec. IV A, we recall that η_{01} can be interpreted as the efficiency of loading the input $s_{\text{in}}(t)$ into Ring 1 before index modulation is applied at time t_1. Hence, from Ref. [28], η_{01} is maximized when $\gamma_{1e} \gg \gamma_0$ and $\gamma_{1e} = k/T_s$ for a constant k of the order of unity, depending on the input pulse shape, e.g. $k = 2.3780$ for the raised cosine [28]. In contrast, η_{12} is maximized with respect to non-negative γ_{1e} when $\gamma_{1e} = 0$. Physically, this is because coupling between the input bus and Ring 1 results only in energy leakage during the energy transfer from Ring 1 to Ring 2. Thus, the partial efficiency $\eta_{02} = \eta_{01}\eta_{12}$ of energy transfer form the input bus to Ring 2 in the limit $|\Delta_0| \to \infty$ (and hence η in this same limit) is maximized with respect to γ_{1e} at some critical value between 0 and k/T_s.

To determine this value, we assume that the ratios $\gamma_j/|\kappa|$ ($j = 1, 2$) are small enough so that the value of γ_{1e} which maximizes η_{02} differs only slightly from k/T_s. Then we may approximate through Taylor polynomials η_{01} as a function of $(\gamma_{1e}T_s - k)$; and η_{12} as a function of $\gamma_j/|\kappa|$. As a result, $\eta_{02} = \eta_{01}\eta_{12}$ can be approximated as as a third-order polynomial in γ_{1e}, which optimum γ_{1e} we can determine analytically. We then use this approximate optimal γ_{1e} as the initial guess of a numerical routine for local optimization. We discuss the details of the polynomial model for η_{02} as a function of γ_{1e} in the Supplemental Material [39].

We evaluate this approach for numerical optimization of η_{02} with respect to γ_{1e}. To do so, we first note that we consider the limit $|\Delta_0| \to \infty$, and that we optimize CAFC with respect to t_1 and t_2 as discussed above in this section. Then we focus on the case of a raised-cosine input of duration T_s and the idealized case of $\gamma_0 = 0$. As in Sec. III, $\gamma_0 = 0$ is chosen for simplicity and to illustrate the fundamental limits of the CAFC efficiency. We illustrate the following analysis of the dependence of η_{02} on γ_{1e} for nonvanishing γ_0 in the Supplemental Material [39], though the qualitative behavior of all quantities is identical for small γ_0. The value of γ_{2e} is set to tune the duration of the CAFC output, as described below in this section. Then η_{02} depends only on two dimensionless products: $\gamma_{1e}T_s$ and $|\kappa|T_s$. Given this observation, we evaluate
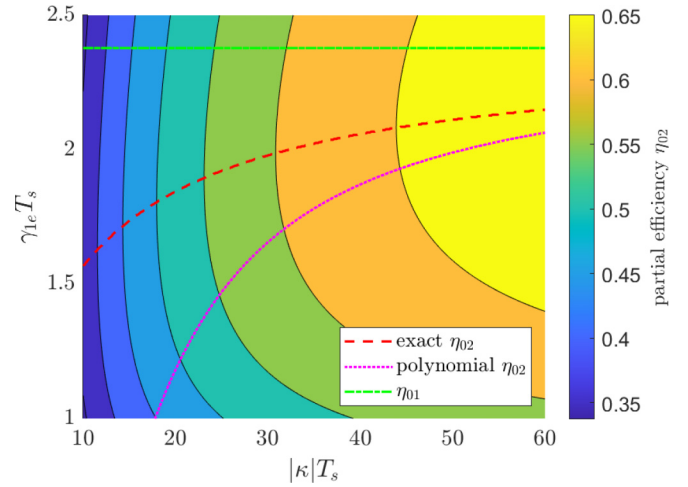

FIG. 3. Contour plot of the maximum partial efficiency η_{02} for $\gamma_0 = 0$ for different values of $|\kappa|T_s$ and $\gamma_{1e}T_s$. Highlighted are also three curves. The first curve corresponds to the value of $\gamma_{1e}T_s$ which maximizes η_{02} for fixed $|\kappa|T_s$ (red). The second and third curves are estimates of the optimal curve. One corresponds to the value of $\gamma_{1e}T_s$ which maximizes the polynomial model for η_{02} (purple), and the other, to the value which maximizes the partial efficiency η_{01} (green).

η_{02} for different values of $\gamma_{1e}T_s$ and $|\kappa|T_s$. We display the results as a contour plot in Fig. 3. In this contour plot, we also trace the curve corresponding to the values of $\gamma_{1e}T_s$ that maximize η_{02} for set values of $|\kappa|T_s$. To compare with this curve, we also highlight two estimates for it. The first estimate is the curve with values of $\gamma_{1e}T_s$ which optimize the aforementioned polynomial model for η_{02} for fixed $|\kappa|T_s$. The second estimate is the curve with values of $\gamma_{1e}T_s$ which optimize η_{01} [28], and are thus constant for all $|\kappa|T_s$, which influences only η_{12}.

We examine the lines of constant $\gamma_{1e}T_s$ and of constant $|\kappa|T_s$ in Fig. 3. For constant $\gamma_{1e}T_s$, η_{02} increases monotonically with $|\kappa|T_s$. This is because, to maximize η_{01}, from the input bus to Ring 1, γ_{1e} must be of the order of T_s^{-1}. Hence, large $|\kappa|T_s$ implies large $|\kappa|/\gamma_{1e}$, and thus small energy leakage during energy transfer from Ring 1 to Ring 2. In contrast, for constant $|\kappa|T_s$, there is always a finite value of $\gamma_{1e}T_s$ which maximizes η_{02}, in agreement with the aforementioned polynomial model for η_{02} and its discussion.

We compare the line of optimal values of $\gamma_{1e}T_s$ with its analytical estimates in Fig. 3. For this comparison, we make three observations. First, the exact optimum value of $\gamma_{1e}T_s$ lies between its two estimates for all of the considered values of $|\kappa|T_s$. This allows us to use these estimates as bounds for the optimum $\gamma_{1e}T_s$ for any $|\kappa|T_s$ for numerical optimization of η_{02}. Second, as $|\kappa|T_s$ increases, the exact optimum $\gamma_{1e}T_s$ converges to its polynomial estimate. This is because then, the interring transfer efficiency η_{12} approaches unity, and its first-order polynomial in $\gamma_j/|\kappa|$ approximates it more accurately. Third, as $|\kappa|T_s$ increases, the polynomial estimate converges to the value which optimizes input loading from the input bus to Ring 1. Again, this is because then η_{01} approaches unity, so $\eta_{02} \approx \eta_{01}$. Then, because the exact optimum $\gamma_{1e}T_s$ is always between these two estimates, it also converges to the value for maximum η_{01}.

Eight, we discuss the effect on the CAFC output of the coupling rate γ_{2e} between Ring 2 and the output bus, and we explain the scheme we use to set is value. In general, varying γ_{2e} has two effects in the CAFC output. First, a change in γ_{2e} alters the CAFC efficiency η. Mainly, this occurs via two competing mechanisms: it decreases the efficiency in energy transfer from Ring 1 to Ring 2 during ring modulation, as energy leaks from Ring 2 into the output bus while the energy in Ring 1 is coupled into Ring 2, which decreases η; also, it increments the energy coupled from Ring 2 into the output bus after modulation, which increases η. Second, an increase in γ_{2e} decreases the duration of the frequency-shifted output pulse. This is because most of the energy of the output is in an exponentially decaying tail of characteristic timescale $1/(2\tilde{\gamma}_2)$ which decreases with increasing γ_{2e}.

We might consider setting γ_{2e} to the value which maximizes the η. Nonetheless, determining this optimal value of γ_{2e} is challenging. For simplicity, we may consider η in the limit $|\Delta_0| \to \infty$, where η becomes expressible as the product of the partial efficiencies $\eta_{j,j+1}$ ($j = 0, 1, 2$). Even then, the problem remains formidable. However, if we assume that the interring coupling strength $|\kappa|$ is large compared to the ring decay rates γ_j ($j = 1, 2$), we may approximate the partial efficiency $\eta_{12} = |u_{21}(t_*, 0)|^2$ by a Taylor polynomial. Then, we may analytically optimize the partial efficiency $\eta_{13} = \eta_{12}\eta_{23}$. This is analogous to how we set γ_{1e} by optimizing $\eta_{02} = \eta_{01}\eta_{12}$.

Nonetheless, optimizing η with respect to γ_{2e} in the limits $|\Delta_0| \to \infty$ and $\gamma_j/|\kappa| \to 0$ yields a value of γ_{2e} that depends on γ_{1e}. Conversely, optimizing η similarly with respect to γ_{1e} yields a value of γ_{1e} that depends on γ_{2e}. Thus, the problem of optimizing η with respect to both rates simultaneously, even under these approximations, becomes a challenging set of simultaneous nonlinear equations, which requires numerical solution. Even obtaining initial estimates for the optimal γ_{1e} and γ_{2e} proves difficult.

To circumvent the formidable numerical problem of optimizing η with respect to γ_{2e}, we neglect the effect of γ_{2e} on η, and we rather engineer its effect on the output pulse duration. As we discuss in the Supplemental Material [39], this neglect is accurate for small $\gamma_{2e}/|\kappa|$. Explicitly, we set γ_{2e} so that the frequency-shifted output $s_{\text{out}}(t)$ has a root-mean-square (RMS) duration T_{RMS} approximately equal to that of the input $s_{\text{in}}(t)$. Consequently, the frequency-shifted $s_{\text{out}}(t)$ shall have a bandwidth comparable to that of $s_{\text{in}}(t)$, in the order of $2\pi/T_{\text{RMS}}$. Our scheme used to accomplish this is discussed further in the Supplemental Material [39].

To close this section, we briefly discuss the extension of our optimization scheme for N-ring CAFC with $N > 2$. Most of the results of this section still hold for the N-ring system, albeit with the following small modifications. First, we note that the middle rings [with index j, such that $2 \leqslant j \leqslant (N-1)$], have no extrinsic loss γ_{je}, as they are not coupled to the input or output buses. They have only intrinsic loss γ_0. Hence the interring coupling $|\kappa|$ among them need only be large enough so $\gamma_0 \ll |\kappa|$ to inhibit loss during interring energy exchange. In turn, this looser requirement on the interring coupling allows interring leakage due to finite $|\kappa/\Delta_0|$ to be smaller for a fixed value of $|\Delta_0|$. By adding additional rings to the system, one must optimize the efficiency η over the

durations $(t_{j+1} - t_j)$ of the intermediate ring modulations. These must maximize interring energy transfer, just as the single modulation duration $(t_2 - t_1)$ of the two-ring system. To zeroth order in γ_0, the optimal durations $(t_{j+1} - t_j)$ equal $\pi/(2|\kappa|)$. For exact, and higher-order, expressions, see the Supplemental Material [39]. Finally, we note that for $N > 2$, there is no first-neighbor coupling between Ring 1 and Ring N, the two rings coupled to waveguide buses and hence with nonzero extrinsic loss. Thus, independent optimization of η with respect to γ_{1e} and γ_{2e} is more accurate for finite interring detuning $|\Delta_0|$, as they become increasingly decoupled as the number of rings, N, increases.

VI. CONVERGENCE ANALYSIS OF THE CAFC EFFICIENCY

With the scheme of Sec. V, we optimize CAFC with respect to most of the process's timescales. In particular, we explain in that section that the CAFC efficiency increases as $\gamma_0 T_s$ tends to zero, and as $|\kappa|T_s$ and $|\Delta_0/\kappa|$ tend to infinity. In practice, these three dimensionless parameters have finite, nonzero values; so it is important to analyze how quickly the CAFC efficiency η converges to its maximum with respect to them and, of course, the numerical value of this maximum. As we show in Sec. VII, this analysis allows us to develop an accurate, simple polynomial model of the dependence of η on these three dimensionless parameters. We may then use this polynomial model to estimate optimal values for the remaining free TCMT timescales (e.g., the interring coupling rate $|\kappa|$, and possibly the pulse duration T_s) and the scaling of η with the interring detuning $|\Delta_0|$. Furthermore, we show in this section that our CAFC scheme converges to the same maximum as single-ring AFC [28]. This is a key result because, as we discuss below, it directly implies there exist conditions under which CAFC can be more efficient than multiple instances of single-ring AFC in series.

We start by examining the convergence of η with respect to the normalized interring detuning $|\Delta_0/\kappa|$. As stated previously, efficient CAFC requires this ratio to be large, so the input pulse $s_{\text{in}}(t)$ can be efficiently loaded from the input bus into Ring 1 without leaking into Ring 2, and so the frequency-shifted output $s_{\text{out}}(t)$ can efficiently exit from Ring 2 into the output bus without leaking into Ring 1. As stated in the previous paragraph, η depends on the three dimensionless parameters $|\Delta_0/\kappa|$, $|\kappa|T_s$, and $\gamma_0 T_s$. Hence, we analyze the rate of convergence of η with respect to $|\Delta_0/\kappa|$ as a function of two independent variables: $|\kappa|T_s$ and $\gamma_0 T_s$. First, we take $\gamma_0 T_s$ as constant, and examine the rate of convergence of η with respect to $|\Delta_0/\kappa|$ for different values of $|\kappa|T_s$. Then we take $|\kappa|T_s$ as constant, and consider different values of $\gamma_0 T_s$. Finally, we draw general conclusions by varying both $|\kappa|T_s$ and $\gamma_0 T_s$ simultaneously.

The numerical results of this convergence analysis are shown in Fig. 4. In Fig. 4(a) we study the convergence of η with respect to $|\Delta_0/\kappa|$ for $\gamma_0 T_s = 0$ and different values of $|\kappa|T_s$. To aid visualization and subsequent discussion, Fig. 4(a) also shows $\eta_0 = \lim_{|\Delta_0| \to \infty} \eta$ (as introduced in Sec. IV A) for $\gamma_0 T_s = 0$ and each value of $|\kappa|T_s$. We verify that, for all values of $|\kappa|T_s$, η indeed converges to η_0 as $|\Delta_0/\kappa|$ increases. Moreover, we observe in Fig. 4(a) that η converges to η_0
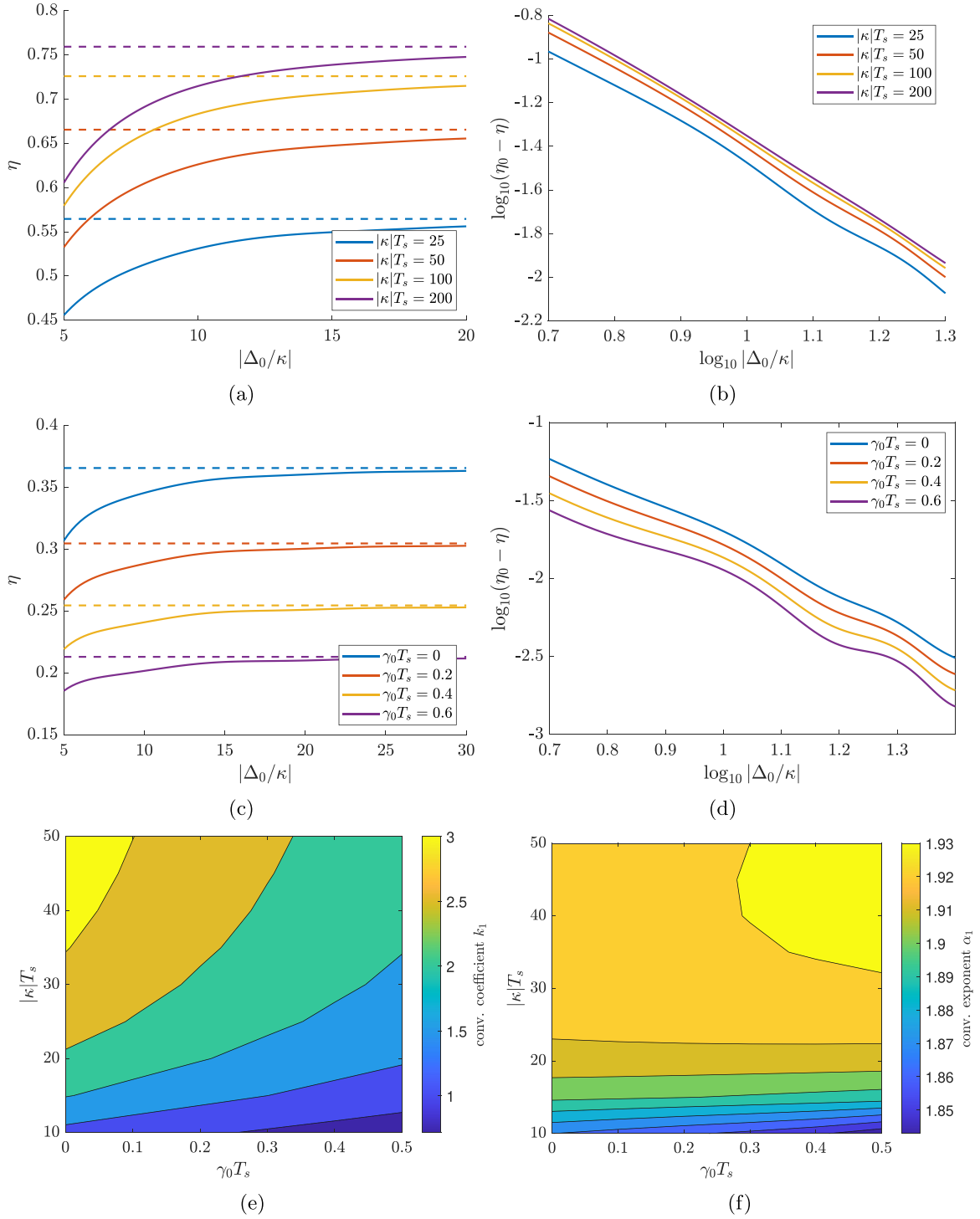
FIG. 4. Numerical analysis of the rate of convergence of the CAFC efficiency η with respect to the normalized interring detuning $|\Delta_0/\kappa|$ to its infinite-detuning value, η_0: (a) η as a function of $|\Delta_0/\kappa|$ and its limit η_0 for $\gamma_0 T_s = 0$ and different $|\kappa|T_s$; (b) $\log_{10}(\eta_0 - \eta)$ as a function of $\log_{10}|\Delta_0/\kappa|$ for $\gamma_0 T_s = 0$ and different $|\kappa|T_s$; (c) η as a function of $|\Delta_0/\kappa|$ and its limit η_0 for $|\kappa|T_s = 10$ and different $\gamma_0 T_s$; (d) $\log_{10}(\eta_0 - \eta)$ as a function of $\log_{10}|\Delta_0/\kappa|$ for $|\kappa|T_s = 10$ and different $\gamma_0 T_s$; (e) estimate of the convergence coefficient k_1 as a function of $|\kappa|T_s$ and $\gamma_0 T_s$; (f) estimate of the convergence exponent α_1 as a function of $|\kappa|T_s$ and $\gamma_0 T_s$.

monotonically from below for all considered values of $|\Delta_0/\kappa|$. This observation suggests that η_0 is indeed an upper bound on η for large, finite $|\Delta_0/\kappa|$, provided the remaining TCMT parameters remain fixed. Of course, we expect this to be the case for sufficiently large $|\Delta_0/\kappa|$, based on the discussion of

the role of $|\Delta_0|$ in Sec. V. Furthermore, we observe in Fig. 4(a) that both η for finite $|\Delta_0|$ and its limit η_0 for infinite $|\Delta_0|$ increase monotonically with $|\kappa|T_s$. This monotonic increase with $|\kappa|T_s$ agrees with the discussion in Sec. V. There we explained that increasing $|\kappa|T_s$ enables larger ratios of $|\kappa|$ to

the optimal bus-ring coupling rates γ_{1e} and γ_{2e}, reducing the energy dissipated in transferring energy from Ring 1 to Ring 2 during ring modulation.

We examine the convergence of η with respect to $|\Delta_0/\kappa|$. To do so, we evaluate the difference between η and its value in the limit of infinite interring detuning, η_0. We surmise that $(\eta_0 - \eta)$ scales approximately as a positive power of $|\kappa/\Delta_0|$ for sufficiently large $|\Delta_0/\kappa|$. To test this hypothesis, we plot the logarithm of $(\eta_0 - \eta)$ against that of $|\Delta_0/\kappa|$ for $\gamma_0 T_s = 0$ and different values of $|\kappa| T_s$ in Fig. 4(b). From this figure, we observe that the relation between $\log_{10}(\eta_0 - \eta)$ and $\log_{10}|\Delta_0/\kappa|$ is approximately linear, with negative slope, for all values of $|\kappa| T_s$. This implies that $(\eta_0 - \eta)$ is indeed approximately proportional to a positive power of $|\kappa/\Delta_0|$, for large $|\Delta_0/\kappa|$. We note that the curves in Fig. 4(b) all have approximately the same slope, which implies $(\eta_0 - \eta)$ is approximately proportional to the same power of $|\kappa/\Delta_0|$, for all considered values of $|\kappa| T_s$.

Next, we analyze the convergence of η with respect to $|\Delta_0/\kappa|$ for different values of $\gamma_0 T_s$ and constant $|\kappa| T_s$. Thus, in analogy to Fig. 4(a), we plot η and its limit η_0 as a function of $|\Delta_0/\kappa|$ for different values of $\gamma_0 T_s$ and large, fixed $|\kappa| T_s$, specifically, $|\kappa| T_s = 10$. The result is shown in Fig. 4(c). The qualitative behavior of η in Fig. 4(c) is similar to that in Fig. 4(a). Explicitly, η grows monotonically with $|\Delta_0/\kappa|$, converging to η_0 from below for each value of $\gamma_0 T_s$. As expected, as $\gamma_0 T_s$ increases, both η and η_0 decrease, as then more energy is dissipated into the environment during the CAFC process. Again, we surmise there is a power law relating $(\eta_0 - \eta)$ to $|\Delta_0/\kappa|$ for sufficiently large $|\Delta_0/\kappa|$. To test this claim, we again plot $(\eta_0 - \eta)$ against $|\Delta_0/\kappa|$ in a logarithmic scale. The result is in Fig. 4(d). As Fig. 4(b), Fig. 4(d) confirms an approximate linear relation between the logarithms of $(\eta_0 - \eta)$ and $|\Delta_0/\kappa|$ and thus a power law between them, now for all considered values of $\gamma_0 T_s$. Again, we note that the curves in the logarithmic plot of Fig. 4(d) have approximately the same slope. Hence, $(\eta_0 - \eta)$ is proportional to the same power of $|\Delta_0/\kappa|$, independently of $\gamma_0 T_s$

Having confirmed numerically the existence of an approximate power law for $(\eta_0 - \eta)$ as a function of $|\Delta_0/\kappa|$, we next characterize it quantitatively. To do so, based on the observations of this section, we approximate η as a function of $|\Delta_0/\kappa|$ via

$$\eta \approx \eta_0 - k_1 \left| \frac{\kappa}{\Delta_0} \right|^{\alpha_1} \quad \text{for } |\Delta_0| \gg |\kappa|. \tag{28}$$

In Eq. (28) we introduce the convergence coefficient k_1, and the convergence exponent α_1. Because η depends on $|\Delta_0/\kappa|$, $|\kappa| T_s$, and $\gamma_0 T_s$, k_1 and α_1 generally depend on $|\kappa| T_s$ and $\gamma_0 T_s$. We then estimate k_1 and α_1 as functions of $|\kappa| T_s$ and $\gamma_0 T_s$. We estimate them via linear regression of $\log_{10}(\eta_0 - \eta)$ as a function of $\log_{10}|\Delta_0/\kappa|$ based on a least mean squares criterion, for different values of $|\kappa| T_s$ and $\gamma_0 T_s$.

In Figs. 4(e) and 4(f), we show contour plots of the resulting estimates of k_1 and α_1, respectively, as functions of $|\kappa| T_s$ and $\gamma_0 T_s$. In Fig. 4(e), the convergence coefficient k_1 exhibits large relative change with these parameters, varying from 1 to 3. For small $|\kappa| T_s$ (less than 20), k_1 is approximately

independent of $\gamma_0 T_s$. But as $|\kappa| T_s$ grows, k_1 increases and so does its susceptibility to $\gamma_0 T_s$. In contrast, the convergence exponent α_1 exhibits small relative change, in Fig. 4(f) varying from 1.85 to 1.93. In Fig. 4(f), α_1 appears more sensitive to $|\kappa| T_s$ than to $\gamma_0 T_s$. Though the relative variation of α_1 with respect to $|\kappa| T_s$ is still appreciably small.

Next, we study the dependence of the value η_0 of the CAFC efficiency η in the limit of infinite interring detuning $|\Delta_0|$. The limiting value η_0 itself depends on the dimensionless products $|\kappa| T_s$ and $\gamma_0 T_s$, converging to a finite maximum as $|\kappa| T_s \to \infty$, and $\gamma_0 T_s \to 0$. For simplicity of the subsequent analysis, we examine first the convergence of η_0 with respect to $|\kappa| T_s$, and then the convergence of the resulting limit with respect to $\gamma_0 T_s$. From Sec. IV A, we recall that the limit η_0 is expressible as the product of three partial efficiencies $\eta_{j,j+1}$ ($j = 0, 1, 2$). Furthermore, the partial efficiency η_{23} (of the energy release from Ring 2 into the output bus) is independent of $|\kappa| T_s$ for our CAFC scheme. Thus, we need only consider the convergence of the partial efficiency $\eta_{02} = \eta_{01}\eta_{12}$ with respect to $|\kappa| T_s$ to analyze that of η_0, i.e., the efficiency of the complete CAFC process.

Thus, we analyze numerically the convergence of η_{02} as $|\kappa| T_s$ diverges for several values of $\gamma_0 T_s$. To do this, we study the plots in Fig. 5. In Fig. 5(a), in particular, we observe η_{02} converges with respect to $|\kappa| T_s$, similarly to how η converges with respect to $|\Delta_0/\kappa|$ in Figs. 4(a) and 4(c). Explicitly, η_{02} increases monotonically with $|\kappa| T_s$, converging to a finite limit below unity, depending on the value of $\gamma_0 T_s$. In particular, we find that the limiting value of η_{02} for infinite $|\kappa| T_s$ equals the partial efficiency η_{01}, maximized over the input bus-Ring 1 coupling γ_{1e} and and the modulation start time t_1 for the corresponding value of $\gamma_0 T_s$. This limiting value for η_{02} is intuitive. When $\gamma_0 T_s$ is small, and $|\kappa|$ is large compared to T_s^{-1}, $|\kappa|$ is large compared to γ_1 and γ_2. Then the energy exchange between Ring 1 and Ring 2 is nearly lossless, so $\eta_{12} \approx 1$ and $\eta_{02} \approx \eta_{01}$.

As in our discussion of Fig. 4, we surmise that there might be a power law describing the convergence of η_{02} with respect to $|\kappa| T_s$ observed in Fig. 5(a). To test this hypothesis, we consider the difference $(\eta_{01} - \eta_{02})$ between η_{02} and its limiting efficiency η_{01}, and we again plot $\log_{10}(\eta_{01} - \eta_{02})$ against $\log_{10}(|\kappa| T_s)$ in Fig. 5(b). Again, we confirm from Fig. 5(b) that the relation between these logarithms is approximately linear for all considered values of $\gamma_0 T_s$. Moreover, the relation between $(\eta_{01} - \eta_{02})$ and $|\kappa| T_s$ appears approximately equal for all values of $\gamma_0 T_s$. Thus, the most notable effect of $\gamma_0 T_s$ on η_{02} is to change η_{01}, i.e., its limit for infinite $|\kappa| T_s$.

Next, we leverage the apparent power law from Fig. 5(b) between $(\eta_{01} - \eta_{02})$ and $|\kappa| T_s$ to quantitatively characterize the rate of convergence of η_{02} with respect to $|\kappa| T_s$. Thus, we model the dependence of η_{02} on $|\kappa| T_s$ as

$$\eta_{02} \approx \eta_{01} - k_2 (|\kappa| T_s)^{-\alpha_2}, \quad \text{for } |\kappa| \gg T_s^{-1}, \tag{29}$$

for some convergence coefficient k_2, and a convergence exponent α_2. Because η_{02} is a function of $|\kappa| T_s$ and $\gamma_0 T_s$, k_2 and α_2 are functions of $\gamma_0 T_s$. As for k_1 and α_1 in Eq. (28), we estimate k_2 and α_2 through linear regression of $\log_{10}(\eta_{01} - \eta_{02})$ as a function of $\log_{10}(|\kappa| T_s)$ for different values of $\gamma_0 T_s$. The resulting estimates for k_2 and α_2 are shown in Fig. 5(c). We confirm that both k_2 and α_2 exhibit small relative change for
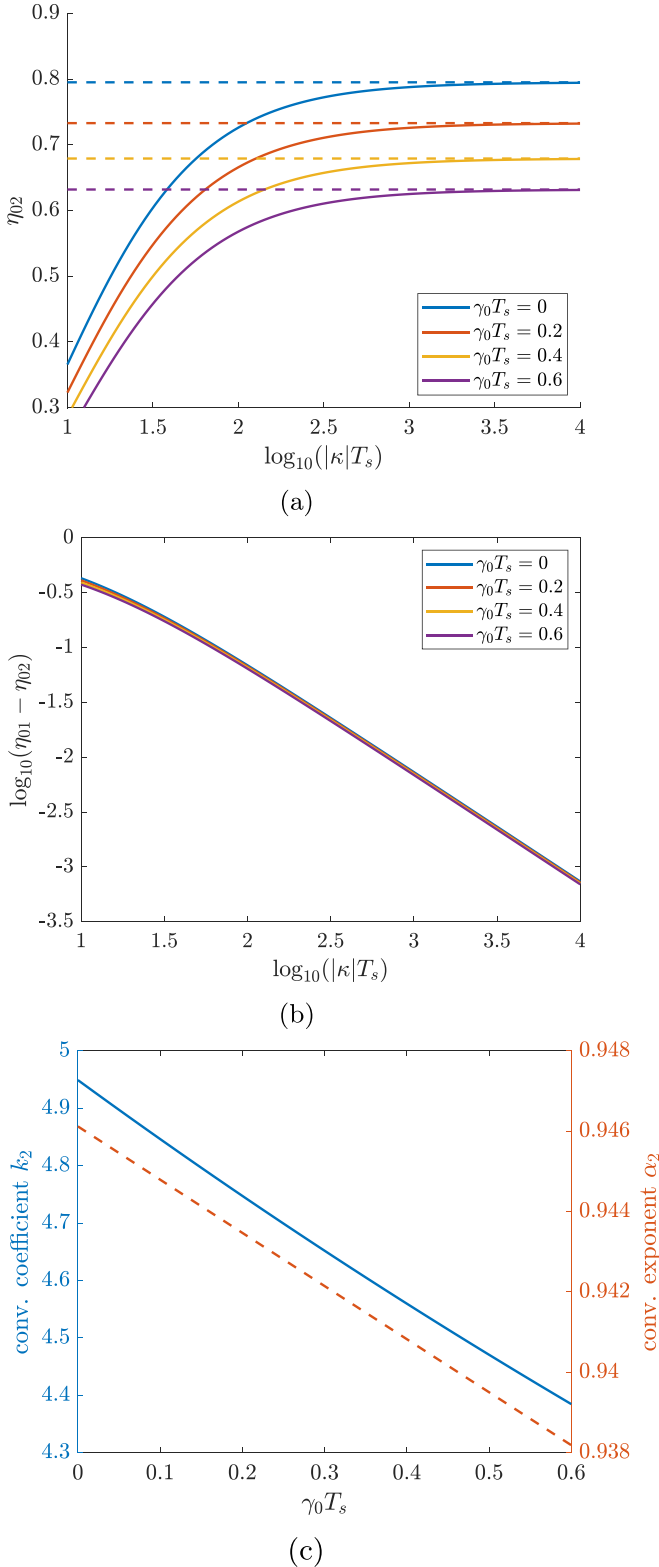
(a)

(b)

(c)

FIG. 5. Numerical analysis of the rate of convergence of the partial CAFC efficiency η_{02} with respect to the normalized interring coupling $|\kappa|T_s$ to the partial efficiency η_{01}: (a) η_{02} as a function of $\log_{10}(|\kappa|T_s)$ and its limit η_{01} for different $\gamma_0 T_s$; (b) $\log_{10}(\eta_{01} - \eta_{02})$ as a function of $\log_{10}(|\kappa|T_s)$ for different $\gamma_0 T_s$; (c) estimates of the convergence coefficient k_2 and of the convergence exponent α_2 as functions of $\gamma_0 T_s$.
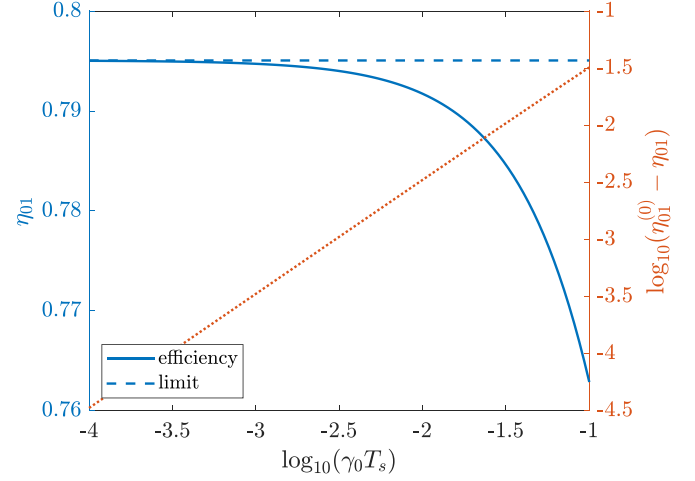

FIG. 6. Numerical analysis of the rate of convergence of the partial CAFC efficiency η_{01} with respect to the normalized intrinsic loss $\gamma_0 T_s$ to its maximum $\eta_{01}^{(0)}$. Depicted are η_{01} (solid blue line), $\eta_{01}^{(0)}$ (dashed blue lined), and $\log_{10}(\eta_{01}^{(0)} - \eta_{01})$ (dotted orange line).

the considered values of $\gamma_0 T_s$, as expected from our discussion of Fig. 5(b). The convergence coefficient k_2 goes from 4.95 at $\gamma_0 T_s = 0$ to 4.40 for $\gamma_0 T_s$. Conversely, the convergence exponent α_2 decreases from 0.946 at $\gamma_0 T_s = 0$ to 0.938 at $\gamma_0 T_s = 0.6$. Both parameters change approximately linearly with $\gamma_0 T_s$.

To complete our convergence analysis, we next examine how the partial efficiency η_{01} converges to its maximum as $\gamma_0 T_s$ tends to zero. As mentioned in this section, and as follows from Eq. (25) in Sec. IV A, η_{01} is the efficiency with which the input pulse $s_{\text{in}}(t)$ in the input bus is loaded into Ring 1, isolated from Ring 2 due to the large interring detuning. We recall that, for each value of $\gamma_0 T_s$, the input coupling γ_{1e} and the modulation time t_1 are chosen to maximize η_{01}. For $\gamma_0 = 0$, we have $\gamma_{1e} = \gamma_1$, and then η_{01} from Eq. (25) reduces to the squared modulus of the projection of $s_{\text{in}}(t)$ onto n_{in} (the time-reversed impulse response of Ring 1), normalized to the input energy $\langle s_{\text{in}}(t)|s_{\text{in}}(t)\rangle$. For $\gamma_0 = 0$, the loading efficiency η_{01} is then identical to the efficiency of single-ring AFC at time $t = t_1$ (also with vanishing intrinsic loss) [28]. In Ref. [28] we found that single-ring AFC efficiency for a raised-cosine input has a maximum of 0.7951 when the input-ring coupling γ_e equals $2.3780 T_s^{-1}$, and modulation is induced at a time $0.2194 T_s$ after the input's maximum. Hence, η_{01} has this same maximum of $\eta_{01}^{(0)} = 0.7951$ under the equivalent conditions $\gamma_{1e} T_s = 2.3780$ and $t_1 = 0.2194 T_s$.

In Fig. 6 we analyze numerically the convergence of the partial efficiency η_{01} to its maximum with respect to $\gamma_0 T_s$. In this plot, we show η_{01} as a function of $\log_{10}(\gamma_0 T_s)$, along with its upper limit of $\eta_{01}^{(0)} = 0.7951$. We verify that η_{01} converges monotonically to $\eta_{01}^{(0)}$ as $\gamma_0 T_s$ decreases for $\log_{10}(\gamma_0 T_s) \leqslant -1$ ($\gamma_0 T_s \leqslant 0.1$). To characterize the rate of convergence, we also plot in Fig. 6 $\log_{10}(\eta_{01}^{(0)} - \eta_{01})$ as a function of $\log_{10}(\gamma_0 T_s)$. Again, we find that the relation between these logarithms is approximately linear. Hence, the convergence of η_{01} to $\eta_{01}^{(0)}$ is well described by a power law for sufficiently small $\gamma_0 T_s$. Then, in analogy to Eqs. (28) and (29), we approximate the

dependence of η_{01} on $\gamma_0 T_s$ as

$$\eta_{01} \approx \eta_{01}^{(0)} - k_3 (\gamma_0 T_s)^{\alpha_3}, \quad \text{for } \gamma_0 \ll T_s^{-1}, \qquad (30)$$

for some convergence coefficient k_3 and convergence exponent α_3. Because η_{01} depends only on $\gamma_0 T_s$, k_3 and α_3 are constant dimensionless parameters. Applying linear regression to the numerical values in Fig. 6, we estimate $k_3 = 0.3259$ and $\alpha_3 = 0.9965$.

Throughout our numerical analysis of the rate of convergence of η with respect to the dimensionless smallness parameters $|\kappa/\Delta_0|$, $(|\kappa|T_s)^{-1}$, and $\gamma_0 T_s$, we identify four recurring features for sufficiently small values of these parameters. These are the following: convergence is always monotonically increasing; convergence is always well described by a power law; the convergence coefficient k_j ($j = 1, 2, 3$) may exhibit significant relative change with the remaining free TCMT parameters, but the convergence exponents α_j do not; and the convergence exponents α_j always take on values slightly smaller than specific integers (either 1 or 2). The fact that η or the corresponding partial efficiency converges monotonically for sufficiently small parameter values agrees with the discussion of Sec. V. There we provided intuitive, physical arguments explaining that we expect η to increase with increasing $|\Delta_0/\kappa|$, increasing $|\kappa|T_s$, and decreasing $\gamma_0 T_s$.

However, the other three observations are new results that cannot be predicted from our previous discussion of the CAFC efficiency η. We interpret these observations as indications that η for our scheme is a smooth function of the three smallness parameters: $|\kappa/\Delta_0|$, $(|\kappa|T_s)^{-1}$, and $\gamma_0 T_s$. Thus, for sufficiently small values of these parameters, η can be accurately approximated through a Taylor polynomial in the smallness paramaters, and then this polynomial dependence dominates the variation of η. In this case, for a given smallness parameter, the corresponding convergence coefficient k_j approximates the coefficient of the Taylor polynomial's lowest-order nonvanishing term and the corresponding convergence exponent α_j, the order of this term. In the Supplemental Material [39], we provide a mathematical argument explaining that the CAFC efficiency of our scheme always is a real analytic (and hence smooth) function of the three smallness parameters, if the input $s_{\text{in}}(t)$ is a complex analytic function of the TCMT parameters.

Given this interpretation of the convergence exponents α_j ($j = 1, 2, 3$) as polynomial-term orders, it is interesting to compare them to each other. From Figs. 4(f) and 5(c), and the value of $\alpha_3 = 0.9965$, the closest integer to α_1 is 2, but the closest integer to α_2 and α_3 is 1. This implies the lowest-order term in the Taylor expansion of η with respect to $(|\kappa|T_s)^{-1}$ and $\gamma_0 T_s$ is of first order, but that with respect to $|\kappa/\Delta_0|$ is of second order. Hence, the implication is that the dependence of η on $|\kappa/\Delta_0|$ vanishes to first order. This result is not obvious from our analysis in the prior sections. But it is consistent with the fact that, for sufficiently large $|\Delta_0|$, Ω_0 varies quadratically with $|\kappa|$, as discussed in the Supplemental Material [39]. In Sec. VII we note that this second-order dependence of η on $|\kappa/\Delta_0|$ modifies the scaling of both the maximum CAFC efficiency η and the conditions required to attain this maximum.

To close this section, we make a key observation from our convergence analysis. This is that the CAFC efficiency η and that of single-ring AFC share the same fundamental tight

upper limit, $\eta_{01}^{(0)}$ of Eq. (30). In other words, the efficiencies of CAFC and single-ring AFC converge towards the same value as they become progressively ideal. This result follows because, in the limit of infinite interring detuning $|\Delta_0|$, η converges to η_0, as implied by Eq. (28). Then, in the limit of infinite normalized interring coupling $|\kappa|T_s$, η_0 converges to $\eta_{01}\eta_{23}$, as implied by Eq. (29). Finally, in the limit of vanishing normalized intrinsic loss, η_{01} converges to $\eta_{01}^{(0)}$, as implied by Eq. (30), and η_{23} converges to unity (see the Supplemental Material [39]), so $\eta_{01}\eta_{23}$ converges to $\eta_{01}^{(0)}$. In summary,

$$\lim_{\substack{|\Delta_0/\kappa| \to \infty \\ |\kappa|T_s \to \infty \\ \gamma_0 T_s \to 0}} \eta = \eta_{01}^{(0)}. \qquad (31)$$

As stated in the discussion of Fig. 6, $\eta_{01}^{(0)}$ is also the value of single-ring AFC in the limit of zero intrinsic loss, i.e., its fundamental tight upper bound.

Equation (31) is a key result of this paper. It implies that, for sufficiently small values of the smallness parameters $|\kappa/\Delta_0|$, $(|\kappa|T_s)^{-1}$, and $\gamma_0 T_s$, the efficiency η of CAFC and that of single-ring AFC can be made arbitrarily close. In particular, it implies that CAFC can be made more efficient than two instances of single-ring AFC in series, which can also induce the same frequency shift of Δ_0 by modulating each ring by $\Delta_0/2$, just as CAFC. To prove that CAFC can become more efficient than serial AFC, we note that in serial AFC, there exists a fundamental mismatch between the output of the first single-ring AFC and the ideal input for the second single-ring AFC. This is because the former is a truncated decaying exponential, and the latter, a truncated increasing exponential [28]. Thus, even for an ideal choice of parameters for the second ring, the second instance of single-ring AFC attains only an energy efficiency of $4e^{-2} \approx 0.5413$ (see the Supplemental Material [39]). Then, so long as the CAFC efficiency is smaller than single-ring AFC efficiency by no more than this factor of $4e^{-2}$, CAFC is more efficient than two instances of single-ring AFC in series.

Though we do not prove it numerically, this result also applies for N-ring CAFC with $N > 2$. In this case, η must still converge polynomially to η_0 of Sec. IV A, as it is still a real-analytic function of the TCMT parameters. Then the N-ring η_0 converges to $\eta_{01}^{(0)}$, as in Eq. (31). This is because the values of η_0 for two-ring CAFC and N-ring CAFC differ only via the partial efficiencies $\eta_{j,j+1}$ [for $j = 1, \ldots, (N-1)$] of the additional stages of interring energy exchange and these all converge to unity as $\gamma_0/|\kappa|$ tends to zero (see Sec. V and the Supplemental Material [39]). Then, the N-ring CAFC efficiency can become arbitrarily close to to $\eta_{01}^{(0)}$, the upper limit for single-ring AFC. Consequently, N-ring CAFC can be more efficient than N instances of single-ring AFC in series, which, at best, have a net efficiency of $\eta_{01}^{(0)}(4e^{-2})^{N-1}$.

VII. MODELING OF THE CAFC EFFICIENCY AS A POLYNOMIAL FUNCTION

In Sec. VI we analyze how the CAFC efficiency η converges monotonically to a maximum as the three normalized smallness parameters $|\kappa/\Delta_0|$, $(|\kappa|T_s)^{-1}$, and $\gamma_0 T_s$ tend to zero. There, we show that the convergence with respect to these parameters is approximately polynomial for sufficiently small

values of these parameters. Thus, in this section, we leverage the results of Sec. VI to model the efficiency η of our scheme as a polynomial function of the smallness parameters. Then we leverage this polynomial model to estimate optimal values of the few remaining free TCMT parameters and to predict scaling laws for these optimal values and for the associated rate of convergence of η.

In the Supplemental Material [39], we argue that the CAFC efficiency η is a smooth function of the smallness parameters. Then we utilize the smoothness of η to approximate it as a Taylor polynomial in these parameters. For simplicity, we consider for this section a fixed normalized intrinsic loss $\gamma_0 T_s$, but variable normalized interring detuning $|\Delta_0/\kappa|$ and normalized interring coupling $|\kappa|T_s$. In practice, this occurs in the case of a fixed intrinsic loss γ_0 and pulse duration T_s, but tunable interring detuning $|\Delta_0|$ and interring coupling $|\kappa|$.

Hence, to lowest order in each of the variable smallness parameters, we write

$$\eta \approx \eta_{01}\eta_{23} - c_1\left|\frac{\kappa}{\Delta_0}\right|^2 - \frac{c_2}{|\kappa|T_s} \quad |\Delta_0| \gg |\kappa|, \quad |\kappa|T_s \gg 1. \tag{32}$$

We recall that η in Eq. (32) is the value of the CAFC efficiency when the constrained TCMT parameters (γ_{1e}, γ_{2e}, t_1, and t_2) are chosen according to our scheme of Sec. V. $\eta_{j,j+1}$ ($j = 0, 1, 2$) are partial CAFC efficiencies in the limit of infinite $|\Delta_0|$, as described in Sec. IV A. Explicitly, η_{01} is the partial efficiency of loading the input $s_{\text{in}}(t)$ into Ring 1, optimized over γ_{1e} and t_1. Conversely, η_{23} is the partial efficiency of loading the frequency-shifted output from Ring 2 into the output bus. For our scheme, η_{23} is given in Sec. V and in the Supplemental Material [39]. In Eq. (32), c_1 and c_2 are positive constant coefficients of the order of unity. These coefficients are related, yet not identical, to the convergence coefficients k_1 and k_2 of Sec. VI, as we discuss below. Because η depends on the normalized intrinsic loss $\gamma_0 T_s$, so do the coefficients c_1 and c_2. In Eq. (32), we take the lowest-order term in $|\kappa/\Delta_0|$ as quadratic, and the one in $(|\kappa|T_s)^{-1}$ as linear. As discussed in the Supplemental Material [39], this choice is made so that the polynomial model reproduces the numerical results of the convergence analysis in Sec. VI, where η converges approximately quadratically with $|\kappa/\Delta_0|$ and approximately linearly with $(|\kappa|T_s)^{-1}$. According to the discussion in the Supplemental Material [39], Eq. (32) is accurate only if $|\Delta_0/\kappa| \gg 1$, and $|\kappa|T_s \gg 1$.

Of course, for Eq. (32) to be useful, we need concrete estimates for the values of $\eta_{01}\eta_{23}$, c_1, and c_2. As noted above, η, and thus $\eta_{01}\eta_{23}$, c_1, and c_2 depend on $\gamma_0 T_s$. So we fix its value to $\gamma_0 T_s = 0.1$ for the subsequent example and the corresponding calculations. The product $\eta_{01}\eta_{23}$ is readily evaluated from the formulas in Sec. IV A, yielding $\eta_{01}\eta_{23} = 0.7413$ for $\gamma_0 T_s = 0.1$. To estimate c_1 and c_2, we evaluate Eq. (32) in the limits of infinite normalized interring detuning $|\Delta_0/\kappa|$ and of infinite normalized interring coupling $|\kappa|T_s$ as

$$\lim_{|\Delta_0/\kappa| \to \infty} \eta \approx \eta_{01}\eta_{23} - \frac{c_2}{|\kappa|T_s},$$

$$\lim_{|\kappa|T_s \to \infty} \eta \approx \eta_{01}\eta_{23} - c_1\left|\frac{\kappa}{\Delta_0}\right|^2. \tag{33}$$

From Eq. (33), c_1 (c_2) is the coefficient of convergence of η with respect to $|\Delta_0/\kappa|$ ($|\kappa|T_s$) in the limit of infinite $|\kappa|T_s$ ($|\Delta_0/\kappa|$). Then we compare Eq. (33) to Eqs. (28) and (29), making the approximation $\alpha_1 = 2$ and $\alpha_2 = 1$. This is justified based on the closeness of the numerically estimated values of α_1 and α_2 to these integers, and on our argument in Sec. VI that η must be a real-analytic function of the smallness parameters. In this way, we relate c_1 and c_2 of Eq. (32) to k_1 and k_2 of Eqs. (28) and (29) in Sec. VI as

$$c_1(\gamma_0 T_s) = \lim_{|\kappa|T_s \to \infty} k_1(|\kappa|T_s, \gamma_0 T_s),$$

$$c_2(\gamma_0 T_s) = \eta_{23}(\gamma_0 T_s)k_2(\gamma_0 T_s). \tag{34}$$

For clarity, in Eq. (34), we explicitly indicate that k_1 of Sec. VI depends on both $|\kappa|T_s$ and $\gamma_0 T_s$, but the remaining quantities (including k_2) depend only on $\gamma_0 T_s$. Following Eq. (34), we immediately estimate c_2 from k_2 at $\gamma_0 T_s = 0.1$ of Sec. VI as $c_2 = 4.7094$. In contrast, we lack an analytical formula to evaluate η in the limit of infinite $|\kappa|T_s$, but finite $|\Delta_0/\kappa|$. Thus, we estimate c_1 as the convergence coefficient k_1 for $\gamma_0 T_s = 0.1$, and the large, but finite, value of $|\kappa|T_s = 50$. In this way, we obtain $c_1 = 3.0050$.

Equation (32) is useful due to its simple and explicit dependence on the smallness parameters $|\kappa/\Delta_0|$ and $(|\kappa|T_s)^{-1}$. This simplicity allows us to estimate optimal values of the remaining free TCMT parameters ($|\kappa|$ in this case of fixed $\gamma_0 T_s$), and predict scaling laws for these optimal values and their associated CAFC efficiency η. The objective of the remainder of this section is to showcase this utility.

First, we leverage Eq. (32) to estimate the optimal interring coupling $|\kappa|$ which maximizes the CAFC efficiency η of our scheme and the corresponding maximum value. To do so, we need only extremize analytically the right-hand side of Eq. (32) with respect to $|\kappa|$, which is straightforward due to its simple polynomial dependence. In this way, we find that η is maximized with respect to $|\kappa|$ when

$$|\kappa| = \kappa_* \approx \left(\frac{c_2}{2c_1}\right)^{1/3}\frac{|\Delta_0|^{2/3}}{T_s^{1/3}}. \tag{35}$$

In Eq. (35) we introduce the critical interring coupling κ_*. When Eq. (35) is satisfied, then Eq. (32) predicts that η approximately equals

$$\eta \approx \eta_{01}\eta_{23}\left[1 - \left(\frac{\Delta_T}{|\Delta_0|}\right)^{2/3}\right]. \tag{36}$$

In Eq. (36), $\Delta_0 T$ is a threshold detuning, given by

$$\Delta_T = \frac{3\sqrt{3}}{2}\frac{T_s^{-1}c_1^{1/2}c_2}{(\eta_{01}\eta_{23})^{3/2}}. \tag{37}$$

Of course, Eq. (36) is accurate only if $|\Delta_0| \gg \Delta_T$. Eqs. (36) and (37) predict that, as the product $|\Delta_0|T_s$ increases, then η (maximized with respect to $|\kappa|$) converges to its upper limit $\eta_{01}\eta_{23}$. This is because, as $|\Delta_0|T_s$ increases, the negative terms in Eq. (32) decrease after maximization with respect to $|\kappa|$.

Next, we validate the accuracy of the analytical estimates of Eqs. (35) and (36) by comparing them with numerical results in Fig. 7. In Fig. 7(a) we show a contour plot of η as a function of $|\Delta_0|T_s$ and $|\kappa|T_s$. In this contour plot, we also plot the analytical estimate for the optimal value $\kappa_* T$ of $|\kappa|T_s$
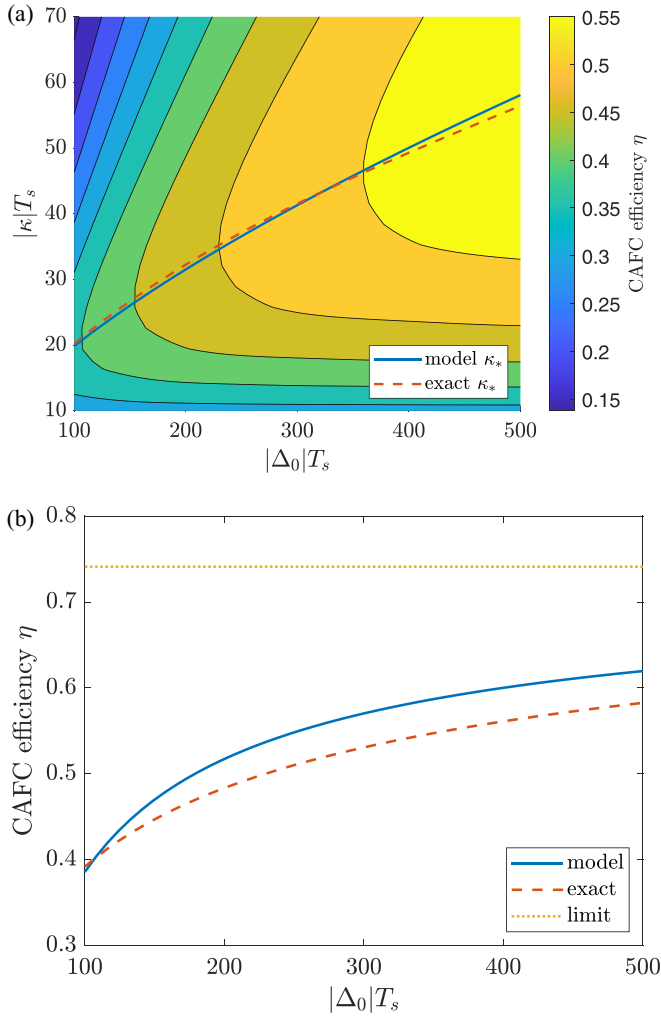
FIG. 7. Comparison of the CAFC efficiency η for $\gamma_0 T_s = 0.1$ as estimated from the polynomial model of Eq. (32) and as obtained via numerical evaluation. (a) Contour plot of η as a function of $|\Delta_0|T_s$ and $|\kappa|T_s$. Also shown are estimates for the optimal value of $|\kappa|$, κ_*, obtained from Eq. (35) and from direct numerical optimization. (b) Plot of the maximized CAFC efficiency η as a function of $|\Delta_0|T_s$, as estimated via the analytical model of Eq. (36) (solid blue line) and via numerical optimization (dashed orange line). Also depicted is the limit $\eta_{01}\eta_{23}$ of η for infinite $|\Delta_0|T_s$.

predicted by Eq. (35), and we compare it with the exact value of $\kappa_* T_s$, obtained via numerical optimization of η with respect to $|\kappa|T_s$. We verify that the analytical and numerical estimates for κ_* remain relatively close for all considered values of $|\Delta_0|T_s$. Furthermore, both the analytical and the numerical estimates for $\kappa_* T_s$ increase similarly with $|\Delta_0|T_s$, proportional to $(|\Delta_0|Ts)^{2/3}$, in agreement with Eq. (35).

In Fig. 7(b) we plot as a function of $|\Delta_0|T_s$ both the analytical estimate from Eq. (36) and the numerical value for the maximum η after it is maximized with respect to $|\kappa|$. For comparison, we also show the value of η in the limit of infinite $|\Delta_0|T_s$, i.e., $\eta_{01}\eta_{23}$. Similarly to the behavior of κ_* in Fig. 7(a), the analytical estimate for the maximized η accurately predicts the numerically exact value and its dependence on $|\Delta_0|T_s$ for all the considered values of $|\Delta_0|T_s$. Hence, we verify that

the maximized η for a given value of $|\Delta_0|T_s$ converges to $\eta_{01}\eta_{23}$ approximately according to $(|\Delta_0|T_s)^{-2/3}$, as implied by Eqs. (36) and. (37).

Having verified the accuracy of Eqs. (35) and (36), we next examine their predictions for the scaling of the optimal coupling ratio κ_* and the convergence rate of the optimized η, respectively. Equation (35) predicts the optimal interring coupling κ_* scales as $|\Delta_0|^{2/3}/T_s^{1/3}$; and Eq. (36) predicts the maximized efficiency η converges to $\eta_{01}\eta_{23}$ at a rate proportional to $(|\Delta_0|T)^{2/3}$. These scaling behaviors are a direct consequence of Eq. (32), in particular, of the exponents therein for the smallness parameters $|\kappa/\Delta_0|$ and $(|\kappa|T_s)^{-1}$. Let us compare this to the hypothetical case where the term in Eq. (32) proportional to $|\kappa/\Delta_0|^2$ was instead directly proportional to $|\kappa/\Delta_0|$, i.e., to its first power, rather than the second. In this hypothetical case, it is straightforward to verify that κ_* would scale as $(|\Delta_0|T_s)^{1/2}$, and the maximized η would converge to $\eta_{01}\eta_{23}$ as $(|\Delta_0|T_s)^{-1/2}$. Then the fact that η depends on $|\kappa/\Delta_0|$ only to second order in Eq. (32) qualitatively changes Eqs. (35) and (36). First, it causes the optimal κ_* to increase more rapidly with $|\Delta_0|$ and more slowly with T_s^{-1}. Second, and more importantly, it causes the maximized η to converge to $\eta_{01}\eta_{23}$ more quickly with $|\Delta_0|T_s$.

To highlight the significance of the scaling behavior of the maximized η with $|\Delta_0|T_s$, we provide a sample calculation. In Fig. 7(b) we find that both the analytical and numerical estimates for the maximum η as a function of $|\Delta_0|T_s$ reach a value of approximately 0.6 for $|\Delta_0|T_s = 500$. We assume that the maximized η for fixed $|\Delta_0|T_s$ continues to converge to its maximum $\eta_{01}\eta_{23} = 0.7413$ for $\gamma_0 T_s = 0.1$ at a rate proportional to $(|\Delta_0|T_s)^{-2/3}$, as identified in the previous paragraph. Then, for instance, we immediately deduce from the scaling behavior that a product $|\Delta_0|T_s$ of the order of 3000 is required for η to reach a value of 0.70. Naturally, this assumption on convergence rate is expected to hold. This is because as $|\Delta_0|T_s$ increases, the concomitant optimal values of the smallness parameters $|\kappa/\Delta_0|$ and $(|\kappa|T_s)^{-1}$ decreases, and the polynomial model of Eq. (32) becomes more accurate, as indicated therein and following the discussion of the Supplemental Material [39].

VIII. CONCLUSION

In this paper we proposed and analyzed the energy efficiency of a new photonic circuit and the corresponding modulation scheme for adiabatic frequency conversion (AFC). The circuit consists of a chain of coupled, yet initially detuned ring resonators, coupled at each of its ends to a bus waveguide. The scheme consists of injecting an optical pulse from a bus waveguide into the first ring of the chain, modulating the first pair of rings so they reach resonance and their energies undergo Rabi oscillation, and stopping ring modulation after the energy in the first ring is deposited into the second ring. Then the process is repeated between the second and third ring, and so on. This scheme then realizes cascaded AFC (CAFC), where the output pulse has a frequency shift of N times that applied to the resonance frequency of each ring, where N is the total number of rings in the chain. This CAFC scheme offers the advantage of inducing AFC multiple times in succession without the need to unload the optical pulse into

a bus waveguide between modulations. For concreteness, we examined thoroughly the simplest nontrivial case of a chain of two rings, and briefly discuss the generalization to a chain of arbitrary number of rings.

In the paper we modeled the temporal dynamics of CAFC using temporal coupled mode theory (TCMT), and we proposed a scheme to optimize CAFC practically with respect to the process's timescales. To do so, we first presented the TCMT equations for CAFC and obtained their analytical solution for strong and fast temporal modulation. Then we illustrated the CAFC scheme by discussing in detail a sample CAFC process of a symmetric, single-lobe optical pulse. We analyzed the transformation of the input pulse into the frequency-shifted output as a rank-one linear operator in the vector space of finite-energy pulses. In this way we identified that the CAFC efficiency depends on the input pulse shape through a Schwarz inequality, just as in single-ring AFC. Then we explained the numerical scheme we utilize to practically optimize CAFC process over its multiple timescales. We identified a tight upper bound for the CAFC efficiency under our scheme. We found that this upper bound is identical to that of single-ring AFC, specifically of 0.7951 for a symmetric,

single-lobe input pulse. Consequently, we showed CAFC can become more energy efficient than multiple instances of single-ring AFC in series. We examined how the CAFC efficiency for our scheme converges to its theoretical upper bound as it becomes progressively idealized, as measured by three distinct timescale ratios. We showed that this convergence is polynomial and explained this behavior based on the real analyticity of the CAFC efficiency as a function of its timescales. We leveraged this polynomial convergence to model the CAFC efficiency of our scheme as a polynomial function of the remaining free TCMT parameters. We utilized this polynomial model to optimize our CAFC scheme with respect to the remaining free parameters and to predict its scaling with respect to interring detuning postoptimization.

The CAFC scheme of this work represents then an energy-efficient strategy to extend the frequency shift induced by AFC beyond the limit imposed by the material platform. This broadens the utility of integrated AFC as an alternative for practical frequency shifting of optical signals. This is of technological interest as AFC promises a route towards fully integrated, tunable frequency conversion in the optical regime.

[1] A. C. Turner-Foster, M. A. Foster, R. Salem, A. L. Gaeta, and M. Lipson, Frequency conversion over two-thirds of an octave in silicon nanowaveguides, Opt. Express **18**, 1904 (2010).

[2] Q. Lin, J. Zhang, P. M. Fauchet, and G. P. Agrawal, Ultra-broadband parametric generation and wavelength conversion in silicon waveguides, Opt. Express **14**, 4786 (2006).

[3] W. Mathlouthi, H. Rong, and M. Paniccia, Characterization of efficient wavelength conversion by four-wave mixing in submicron silicon waveguides, Opt. Express **16**, 16735 (2008).

[4] S. Zlatanovic, J. S. Park, S. Moro, J. M. C. Boggio, I. B. Divliansky, N. Alic, S. Mookherjea, and S. Radic, Mid-infrared wavelength conversion in silicon waveguides using ultracompact telecom-band-derived pump source, Nat. Photon. **4**, 561 (2010).

[5] B. E. A. Saleh and M. C. Teich, *Fundamentals of Photonics*, 3rd ed., Wiley Series in Pure and Applied Optics (Wiley, Hoboken, NJ, 2019).

[6] A. Yariv and P. Yeh, *Photonics: Optical Electronics in Modern Communications*, 6th ed., Oxford Series in Electrical and Computer Engineering (Oxford University Press, New York, 2007), pp. 358–380.

[7] R. W. Boyd, *Nonlinear Optics*, 3rd ed. (Academic Press, Amsterdam, 2008), pp. 74–108.

[8] M. F. Yanik and S. Fan, Dynamic photonic structures: Stopping, storage, and time reversal of light, Stud. Appl. Math. **115**, 233 (2005).

[9] M. Notomi and S. Mitsugi, Wavelength conversion via dynamic refractive index tuning of a cavity, Phys. Rev. A **73**, 051803(R) (2006).

[10] W. Pauli, *Statistical Mechanics*, Pauli Lectures on Physics (Dover Publications, Mineola, NY, 1973), pp. 85–87.

[11] H. Goldstein, C. Poole, and J. Safko, *Classical Mechanics*, 3rd ed. (Addison-Wesley, San Francisco, 2002), pp. 549–553.

[12] S. F. Preble, Q. Xu, and M. Lipson, Changing the colour of light in a silicon resonator, Nat. Photon. **1**, 293 (2007).

[13] S. Preble, L. Cao, A. Elshaari, A. Aboketaf, and D. Adams, Single photon adiabatic wavelength conversion, Appl. Phys. Lett. **101**, 171110 (2012).

[14] T. Tanabe, M. Notomi, H. Taniyama, and E. Kuramochi, Dynamic release of trapped light from an ultrahigh-Q nanocavity via adiabatic frequency tuning, Phys. Rev. Lett. **102**, 043907 (2009).

[15] R. Konoike, H. Nakagawa, M. Nakadai, T. Asano, Y. Tanaka, and S. Noda, On-demand transfer of trapped photons on a chip, Sci. Adv. **2**, e1501690 (2016).

[16] T. Tanabe, E. Kuramochi, H. Taniyama, and M. Notomi, Electro-optic adiabatic wavelength shifting and Q switching demonstrated using a p-i-n integrated photonic crystal nanocavity, Opt. Lett. **35**, 3895 (2010).

[17] N. Karl, P. P. Vabishchevich, M. R. Shcherbakov, S. Liu, M. B. Sinclair, G. Shvets, and I. Brener, Frequency conversion in a time-variant dielectric metasurface, Nano Lett. **20**, 7052 (2020).

[18] W. Yoshiki, Y. Honda, M. Kobayashi, T. Tetsumoto, and T. Tanabe, Kerr-induced controllable adiabatic frequency conversion in an ultrahigh Q silica toroid microcavity, Opt. Lett. **41**, 5482 (2016).

[19] Y. Minet, L. Reis, J. Szabados, C. S. Werner, H. Zappe, K. Buse, and I. Breunig, Pockels-effect-based adiabatic frequency conversion in ultrahigh-Q microresonators, Opt. Express **28**, 2939 (2020).

[20] X. He, L. Cortes-Herrera, K. Opong-Mensah, Y. Zhang, M. Song, G. P. Agrawal, and J. Cardenas, Electrically induced adiabatic frequency conversion in an integrated lithium niobate ring resonator, Opt. Lett. **47**, 5849 (2022).

[21] Y. Xiao, G. P. Agrawal, and D. N. Maywar, Spectral and temporal changes of optical pulses propagating through time-varying linear media, Opt. Lett. **36**, 505 (2011).

[22] Y. Xiao, D. N. Maywar, and G. P. Agrawal, Optical pulse propagation in dynamic Fabry–Perot resonators, J. Opt. Soc. Am. B **28**, 1685 (2011).

[23] B. A. Daniel, D. N. Maywar, and G. P. Agrawal, Dynamic mode theory of optical resonators undergoing refractive index changes, J. Opt. Soc. Am. B **28**, 2207 (2011).

[24] M. Minkov, Y. Shi, and S. Fan, Exact solution to the steady-state dynamics of a periodically modulated resonator, APL Photonics **2**, 076101 (2017).

[25] M. Minkov and S. Fan, Localization and time-reversal of light through dynamic modulation, Phys. Rev. B **97**, 060301(R) (2018).

[26] M. R. Shcherbakov, P. Shafirin, and G. Shvets, Overcoming the efficiency-bandwidth tradeoff for optical harmonics generation using nonlinear time-variant resonators, Phys. Rev. A **100**, 063847 (2019).

[27] B. A. Daniel, D. N. Maywar, and G. P. Agrawal, Efficient adiabatic wavelength conversion in Gires–Tournois resonators, Opt. Lett. **36**, 4155 (2011).

[28] L. Cortes-Herrera, X. He, J. Cardenas, and G. P. Agrawal, Optimization of adiabatic frequency conversion in an all-pass resonator, Phys. Rev. A **106**, 023517 (2022).

[29] H. A. Haus, *Waves and Fields in Optoelectronics*, Prentice-Hall Series in Solid State Physical Electronics (Prentice-Hall, Englewood Cliffs, NJ, 1984).

[30] B. E. Little, S. T. Chu, H. A. Haus, J. Foresi, and J.-P. Laine, Microring resonator channel dropping filters, J. Lightwave Technol. **15**, 998 (1997).

[31] C. Manolatou, M. Khan, S. Fan, P. R. Villeneuve, H. Haus, and J. Joannopoulos, Coupling of modes analysis of resonant channel add-drop filters, IEEE J. Quantum Electron. **35**, 1322 (1999).

[32] J. D. Joannopoulos, S. G. Johnson, J. N. Winn, and R. D. Meade, *Photonic Crystals: Molding the Flow of Light*, 2nd ed. (Princeton University Press, Princeton, 2008).

[33] V. Van, *Optical Microring Resonators*, Series in Optics and Optoelectronics (CRC Press, Boca Raton, FL, 2016).

[34] A. Papoulis, Maximum response with input energy constraints and the matched filter principle, IEEE Trans. Circuit Theory **17**, 175 (1970).

[35] A. Papoulis, *Signal Analysis* (McGraw-Hill, New York, 1977).

[36] G. P. Agrawal, *Lightwave Technology: Telecommunication Systems* (Wiley-Interscience, Hoboken, NJ, 2005).

[37] L. Cortes-Herrera, X. He, J. Cardenas, and G. P. Agrawal, Theory of high-efficiency adiabatic frequency conversion in coupled microrings, Phys. Rev. A **108**, 063514 (2023).

[38] M. Zhang, C. Wang, Y. Hu, A. Shams-Ansari, T. Ren, S. Fan, and M. Lončar, Electronically programmable photonic molecule, Nat. Photon. **13**, 36 (2019).

[39] See Supplemental Material at http://link.aps.org/supplemental/10.1103/PhysRevA.109.063510 for detailed mathematical derivations and analyses supporting results in the paper, which include Refs. [40–50].

[40] R. L. Burden and J. D. Faires, *Numerical Analysis*, 8th ed. (Thomson Brooks/Cole, Belmont, CA, 2005).

[41] T. M. Apostol, *Mathematical Analysis*, 2nd ed., Addison-Wesley Series in Mathematics (Addison-Wesley, Reading, MA, 1974).

[42] R. G. Bartle and D. R. Sherbert, *Introduction to Real Analysis*, 4th ed. (Wiley, Hoboken, NJ, 2011).

[43] J. B. Conway, *Functions of One Complex Variable*, 2nd ed., Graduate Texts in Mathematics Vol. 11 (Springer-Verlag, New York, 1978).

[44] J. W. Brown and R. V. Churchill, *Complex Variables and Applications*, 7th ed. (McGraw-Hill Higher Education, Boston, 2004).

[45] E. Freitag and R. Busam, *Complex Analysis*, 2nd ed., Universitext (Springer, Berlin, 2009).

[46] B. C. Hall, *Lie Groups, Lie Algebras, and Representations: An Elementary Introduction*, 2nd ed., Graduate Texts in Mathematics Vol. 222 (Springer, Cham, 2015).

[47] A. Messiah, *Quantum Mechanics* (North-Holland, Amsterdam, 1961).

[48] J. J. Sakurai and J. Napolitano, *Modern Quantum Mechanics*, 2nd ed. (Addison-Wesley, Boston, 2011).

[49] S. G. Krantz and H. R. Parks, *A Primer of Real Analytic Functions*, 2nd ed., Birkhäuser Advanced Texts (Birkhäuser, Boston, 2002).

[50] S. G. Krantz and H. R. Parks, *The Implicit Function Theorem History, Theory, and Applications*, Modern Birkhäuser Classics (Springer, New York, 2013).

[51] S. Hassani, *Mathematical Physics: A Modern Introduction to Its Foundations*, 2nd ed. (Springer International Publishing, Cham, 2013), p. 35.